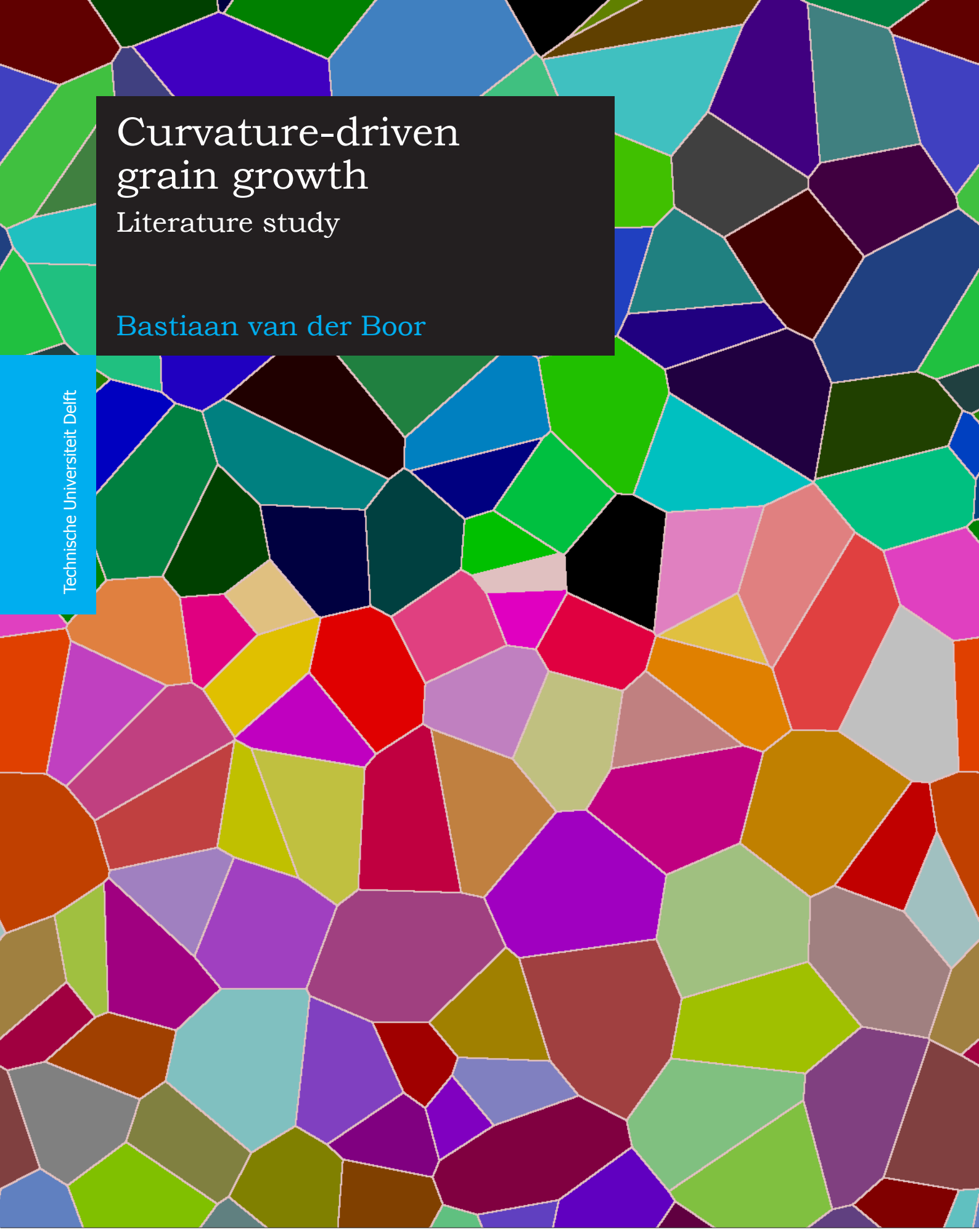

Curvature-driven grain growth

Literature study

Bastiaan van der Boor

Technische Universiteit Delft

TU Delft Delft University of Technology

Challenge the future

Curvature-driven grain growth

Literature study

by

Bastiaan van der Boor

in partial fulfillment of the requirements for the degree of

Master of Science
in Applied Mathematics

at the Delft University of Technology,

Supervisors: dr. ir. F.J. Vermolen, TU Delft
dr. ir. C. Bos, Tata Steel

TU Delft Delft University of Technology

Introduction

Steel is used in numerous products and although already first used in 200 B.C. the development of new kinds of steel has never ceased to stop. More than 30 new kinds of special steel products were developed in the past year at Tata Steel alone, a result of continuous industry demand for improved steel properties. This need for new innovation is mainly driven by the car industry which forms the bulk of Tata Steel customers due to its strategic location in IJmuiden. That is, because car manufacturers in their race to stay ahead of competition, design and produce new car models every year. In order to produce an improved model the lightest, strongest and cheapest steel at that moment available is needed. For R&D researchers this implies a need to getting as fast as possible their products from the drawing board to the customer.

In order to be able to develop new products with certain new properties a lot of prototypes have to be produced based on experience, a time costly process. As the properties of these steels mostly depend on their micro-structure, the process of developing new steels can get more sophisticated when the micro-structure can be better predicted. Therefore a model has been developed by Bos et al. [1] which describes all kinds of metallurgical mechanisms occurring at the production of steel. One important mechanism is currently missing in the model: curvature-driven grain growth.

The goal of this literature study is to explore the theoretical background and methods available to extent the model made by Bos et al. Some methods have been selected and tested on special geometries to make a well founded decision on which method to finally implement in the model of Bos et al [1].

In the first chapter all the necessary background on the metallurgy will be presented to get familiar with all facets that play a role in the micro structure of steel. Next, the most prominent methods to model micro structures will be briefly explained. One of the boundary conditions of this research, is that the method should be implemented in the Cellular Automata method of Bos et al. Therefore each of the reviewed methods to simulate grain growth by curvature in Chapter three are all, at least in theory, possible to implement in the existing model.

Chapter Three first introduces the most intuitive method to calculate the curvature: the counting cell method. Only the principles of this method will be introduced, since it is a very computationally heavy method. Due to observations of Dunn and Chalmers the interests of this thesis will mainly go to vertex methods. One such method that has existed for some time is a method based on the minimization of grain boundary energy. A relatively new method has recently gotten more popular by the extension of the Neumann-Mullins relation in two dimensions in the recently published MacPherson-Srolovitz relation for three dimensions

In Chapter Five some implementation problems are discussed. For example what happens when a grain becomes so small that it disappears. A number of small but very telling test problems are introduced. Finally the results of the methods implemented on these test problems are given. Finally by having reviewed all the literature an informed decision can be made on which method to implement.

Contents

1

Crystal interfaces and micro-structures

In the process of steel making we see a lot of changes happening on a micro-level in the steel. To better understand this process and to see the total effect of each contribution, a model can to be made. We identify three major processes [2] that drive the change in microstructure and need to be taken in consideration when developing the model (where α and β denote in which phase the grains are, note: although they are of the same phase they do not belong to the same grain):

1. Phase-transformation $\alpha - \beta$ interfaces
2. Recrystallization & Recovery $\alpha - \alpha$ interfaces
3. Grain growth $\alpha - \alpha$ interfaces

The first: phase-transformation, generally has the strongest driving force. In steel there are different phases depending on their temperature and carbon concentration. Here a phase corresponds to a certain crystal structure, e.g. how the atoms are arranged. An overview of the phases with the relation to carbon concentration and temperature can be found in the phase diagram, see figure 1.1. Of special interest are the phase transformations occurring when the carbon concentration is around $0.1 - 0.7$ weight percent.

To be considered in this thesis are only two phases: austenite and ferrite. They have the following crystal structure: Face Centered Cubic (FCC) called austenite or Body Centered Cubic (BCC) which is called ferrite. The orientation of the crystal structure can be seen in figure 1.2.

When we look at the phase-diagram it can be seen that depending on temperature and carbon concentration different crystal structures can be observed. Due to geometry of the crystal structure, a considerable amount of carbon can be dissolved. Because carbon atoms are so small such that there is enough space within the structure to fit the atom. When cooling down continues, given a low carbon concentration, the crystal will now transform to a ferrite structure. In this structure less carbon can be dissolved. This seems to contradict that the crystal structure of FCC is more closely packed than BCC, since in FCC 74% of the space is filled in comparison to 68% for BCC. The reason for this seeming discrepancy is that the size of the interstitial gaps in BCC differs, is that it contains a number of small

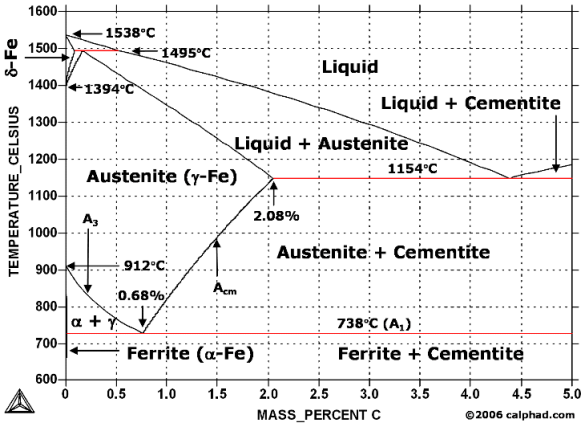

Figure 1.1: Phase diagram, source: [3]

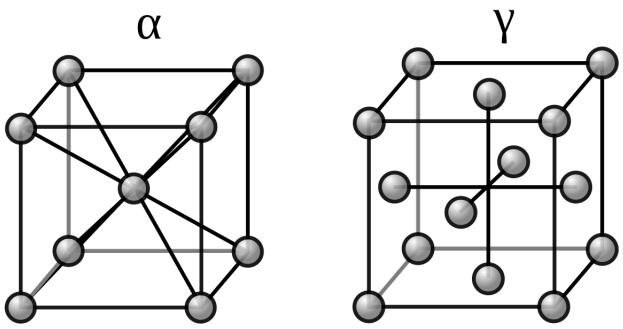

Figure 1.2: Crystal structure of Ferrite BCC α (left) and Austenite FCC γ (right), source: [4]

gaps where the carbon atoms do not fit. Due to this difference in size, the number of gaps, which can contain carbon is larger in FCC than in BCC. This explains the difference in the amount of carbon that can dissolve in each phase.

Second is recrystallization and recovery, which happens simultaneously. Grain growth due to recrystallization is driven by the difference in the density of dislocation between two grains. Dislocations are irregularities in the crystal structure, two basic examples are edge- (see figure 1.3a) and screw dislocations (see figure 1.3b). Recrystallization replaces grains with dislocations by strain-free, or dislocation-free grains. Hence, the dislocations are removed. There now will be places with high dislocation density and where recrystallization has occured a low density of dislocations. Recovery also depends on dislocations, but here dislocations are removed as two dislocations with opposite direction neutralize each other. For an example see figure 1.4. In the first figure on the left as well as on the right there is an edge dislocation. The atoms on the left (green) are situated to near to each other to get the same structure as the lower grain (orange). The other way around is displayed in figure , two dislocations with opposite sign are present. Therefore the dislocation can be removed by recovery, see the middle and lower part of figure 1.4.

Finally, grain growth is considered. This driving force of change will be the main interest of this thesis. Here, the driven force is determined by reduction in grain boundary energy. Further theoretical background explaining the factors which contribute to grain growth will be given in the remaining part

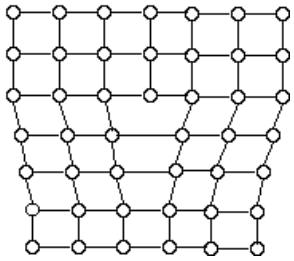

(a) Edge dislocation, source [5]

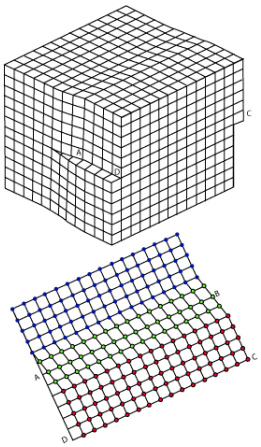

(b) Screw dislocation, source [6]

Figure 1.3: Two examples of dislocations

of this chapter.

1.1. Interfacial free energy

In the past, two different sources of decrease in free energy have been proposed as driving force for grain growth. The first suggestion originally by Czochralski, who proposes a similar idea as used for crystallization [8], is the following: grains formed by recrystallization have a residual strain energy, and that upon further heating the grain with a low residual strain energy will grow at the expense of grains with a high residual strain energy. Ewing and Rosenhain [9] proposed an alternative. They suggested that the interfacial energy of the grain boundaries are the driving force for grain growth. The latter suggestion has been widely accepted as grain boundary melting stops grain growth and therefore disputing the idea of Czochralski. This can be explained as follows: at higher temperature under certain conditions the grain boundaries can melt, meaning that the atoms are no longer ordered in a crystal lattice. Note that this should not effect the growth as the residual strain energy still remains.

From Ewing and Rosenhaim the interfacial free energy is needed to study grain growth. The Gibbs free energy G of a system is given by:

$$G = G_0 + A\gamma. \tag{1.1}$$

Here, G_0 is the energy of the area inside the grain, the second term is the energy contribution of the grain boundary. Further γ is the interfacial free energy per unit area and A denotes the area of the boundary.

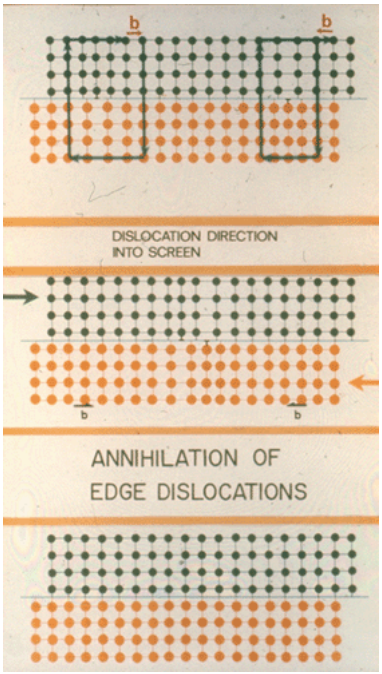

Figure 1.4: Dislocations removed by recovery, source: [7]

The grain boundaries are high-energy regions that increase the free-energy of a polycrystal relative to a single crystal, polycrystalline material is never a true equilibrium structure. Therefore, due to the existence of grain boundaries a metastable equilibrium can be found. This means that a local equilibrium is found. Though, from the definition of metastability, when an activation energy is acquired a new minimum can be found. See figure 1.5 as an illustration.

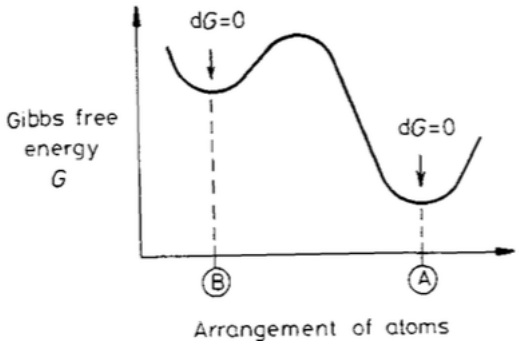

Figure 1.5: Gibbs free energy with two equilibria, source: [2]

1.2. Equivalence to soap froth

From the observation that interfacial free energy must be minimized we can conclude that the driving force is the surface tension of the boundaries. We can defend this as follows. First it is shown by a number of authors that the shape of metal grains is equivalent to the shape of foam cells [10, 11]. Then Smith [12] showed that in a soap foam, surface tension can lead to cell growth that simulates grain growth. From the theory of surface tension which states the Gibbs free energy using the Young-Laplace equation [13]:

$$\Delta G = \gamma V(\frac{1}{R_x} + \frac{1}{R_y}). \tag{1.2}$$

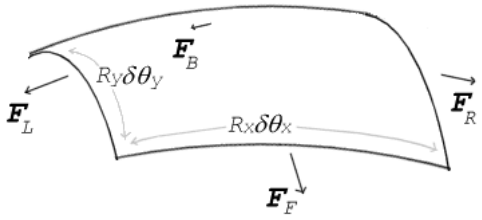

Figure 1.6: Surface tension forces acting on a small surface. $\delta\theta$ and $\delta\theta y$ indicate the amount of bend. Balancing the tension forces with pressure leads to the Young–Laplace equation, source: [14]

The Gibbs free energy depends on γ the grain boundary energy (which will be explained later), V the molar volume and $R_{x,y}$ the radii of curvature of the grains. The grain will be similar to figure 1.6 therefore assume $R_x = R_y$. We have

$$\Delta G = \gamma V(\frac{2}{R_x}). \tag{1.3}$$

It will be assumed that the velocity for grain growth will be proportional to the Gibbs free energy. We arrive at,

$$v = \alpha M \frac{2\gamma}{R_x}, \tag{1.4}$$

where α is a proportionality constant and the M the grain boundary mobility [2].

The condition for the grains to be in equilibrium can be obtained either by considering the total grain boundary energy associated with a particular configuration, or more simply by considering the forces that each boundary exerts on the junction (Chapter 3). Dunn, Chalmers and their co-workers [15, 16] made use of the effect of grain boundary melting on grain growth. They made some interesting observations which strengthens the choice for vertex-based principles. They found when melting a confined region near the grain edges, grain growth will stop. This did not necessarily happen when melting takes place near the center of a grain face. Hence, the effect from curvature near the edges are more pronounced than in the center of grain faces. Therefore, let's now only consider a vertex (intersection of three grains in 2-D).

In the case of a triple point, as the boundary tensions must be in balance, the following must hold for equilibrium:

$$\frac{\gamma_{23}}{\sin\theta_1} = \frac{\gamma_{13}}{\sin\theta_2} = \frac{\gamma_{12}}{\sin\theta_3}. \tag{1.5}$$

When grain boundary energies are assumed to be equal (this assumption will be made clear in the next paragraph). It follows that $\theta_1 = \theta_2 = \theta_3$ and therefore the angle for which the equilibrium holds, $\theta = 120^\circ$ for a triple point. Similarly it can be shown that $\theta = 109.28^\circ$ at a corner where four grains meet in three dimensions.

When these angular conditions are satisfied a complete meta-stable equilibrium is not yet reached. Also the surface tension must balance over all the boundary faces between the junctions. The only way the boundary tension forces can balance in three dimensions is if the boundary is:

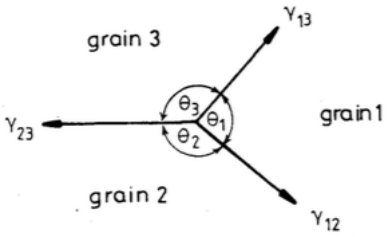

Figure 1.7: The balance of grain boundary tensions for a grain boundary triple point in metastable equilibrium, source: [2]

1. Planar ($r = \infty$) or
2. Curved with equal radii in opposite directions.

Although it is theoretically possible to construct a 3-D polycrystal in which boundary tension forces are in balance, in practice this is not possible. There will always be boundaries with a net curvature in one direction. Some examples of grains with boundary tension forces are given in figure 1.8.

We see that if the number of boundaries is six and if the angles all equal $120°$, the structure is metastable. Because both requisites of metastability are fulfilled: angles and also the edges connecting the vertices are planar. If the number of grain boundaries belonging to one particular grain is smaller than six the edges must be concave, such that the grain will shrink. Opposite, when the number of grain boundaries is larger the grain will grow. This will result in a decrease of the total number of grains and thereby increasing the mean grain size. Hence, the total grain boundary energy is reduced. This phenomenon is known as grain growth or grain coarsening.

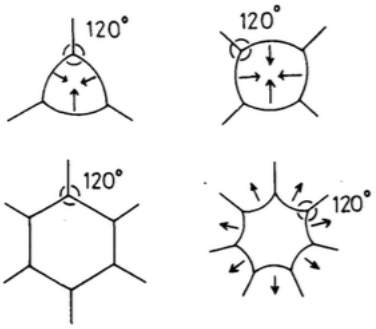

Figure 1.8: Grain boundary configurations all angles are $120°$, source: [2]

1.3. Grain boundary energy

Next the grain boundary energy will be explained. This energy comes from different orientations of a grain around the lattice. By considering two relatively simple orientations the concept will be explained. Two examples are: pure tilt boundaries and pure twist boundaries, see figure 1.9. These lattices of any two grains can be made to coincide by rotating one of them through a suitable angle about a single axis.

To consider the grain boundary energy first the assumption has to be made that the energy is proportional to the dislocations in the boundary. We have,

$$\gamma \propto D_{dis}$$

(a) Tilt (b) Twist

Figure 1.9: Two examples of different orientations, source: [2]

.

Here D_{dis} is the dislocation spacing. The dislocation spacing is calculated with use of the Burgers vector b and the misorientation angle θ:

$$D_{dis} = \frac{b}{\sin\theta} \approx \frac{b}{\theta}$$

.

When first considering a low-angle of misorientation, θ between the two grains. The dislocation spacing is very large and the grain boundary energy γ is approximately proportional to the density of dislocations in the boundary, $1/D_{dis}$.

As θ increases, the strain fields of the dislocations progressively cancel out so γ increases at a decreasing rate. In general when $\theta = 10 - 15°$, the dislocation spacing is so small such that the dislocation cores overlap and it is then impossible to physically identify the individual dislocations. Hence, the grain boundary energy is almost independent of the misorientation! As seen in figure 1.10.

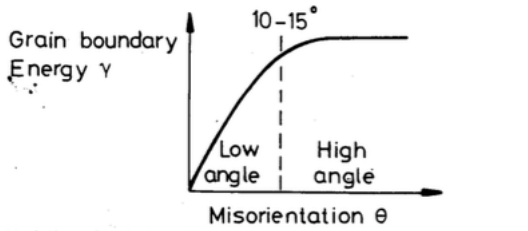

Fig. 3.9 Variation of grain boundary energy with misorientation (schematic).

Figure 1.10: Grain boundary energy depending on the angle of misorientation, source: [2]

1.4. Governing equations

To develop an understanding of curvature driven grain growth a more mathematical approach is needed. To obtain the governing equations used in the modelling the concept of curvature is needed. As seen in equation 1.4 the propagation of the interface depends on the radii of curvature. For any simple closed curve, curvature κ can be calculated for any given point by placing a circle which runs through the point and is tangent to points nearby (see figure 1.11). Now the governing equations of the curvature driven grain growth will be presented. In this report only the curvature flow of planar curves and two dimensional cell structures is considered. In the final report the three dimensional case will be discussed.

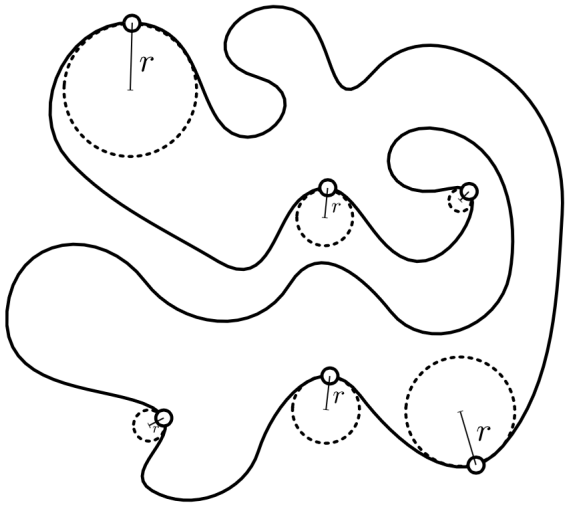

Figure 1.11: A simple, closed curve, with points highlighted, and tangent circles and radii drawn, source: [17]

A curve in the plane can be defined as a continuous mapping $\alpha : I = [a,b] \to \mathbb{R}^2$. The curve is closed if $\alpha(a) = \alpha(b)$, a curve is simple if for all $\hat{s}, u \in (a,b)$, $\alpha(t) \neq \alpha(u)$ (no intersection possible). A curve is regular if $\alpha'(\hat{s}) \neq 0 \ \forall \hat{s} \in I$. The arc-length s of a curve α mapped from the interval $[a,b]$ is defined as $s(\alpha) = \int_a^b |\alpha'(\hat{s})| d\hat{s}$. An arc-length parametrization is chosen such that the arc-length s is always exactly $b - a$.

Let an arc-length parametrized curve α be simple, closed and at least twice differentiable, then $|\alpha'| = 1$ (in higher dimensions $||\nabla\alpha|| = 1$) and curvature κ can be defined as follows. Let $\mathbf{T}(s) = \frac{\alpha'(s)}{||\alpha'(s)||}$ denote the unit tangent to α at a point $\alpha(s)$, pointing in a direction in which the curve is traversed. Let $\mathbf{N}(s)$ be the unit vector normal pointing outwards from α. Let the curve be traversed counterclockwise, then κ is defined as:

$$\kappa = \begin{cases} -||\mathbf{T}'(s)|| = -||\nabla \frac{\nabla\alpha}{||\nabla\alpha||}|| = -||\nabla^2\alpha|| & \text{if the unit tangent vector is turning clockwise} \\ ||\mathbf{T}'(s)|| = ||\nabla \frac{\nabla\alpha}{||\nabla\alpha||}|| = ||\nabla^2\alpha|| & \text{if the unit tangent vector is turning counterclockwise} \end{cases}$$

Let $\alpha(\bullet, 0) : S^1 \to \mathbb{R}^2$ be an embedded, closed planar curve that is at least twice differentiable. Then $\alpha : S^1 \times [0,T] \to \mathbb{R}^2$, where S space has to satisfy:

$$\frac{\partial\alpha}{\partial t} = C\kappa\mathbf{N}, \tag{1.6}$$

as parameter t moves through $[0,T]$ the curve evolves through time. C is a constant which depends on physical properties of the system. An interesting result from Hamilton, Gage, and Grayson [18, 19] which can be observed in figure 1.12 is that every curve will finally evolve to a circle as it shrinks.

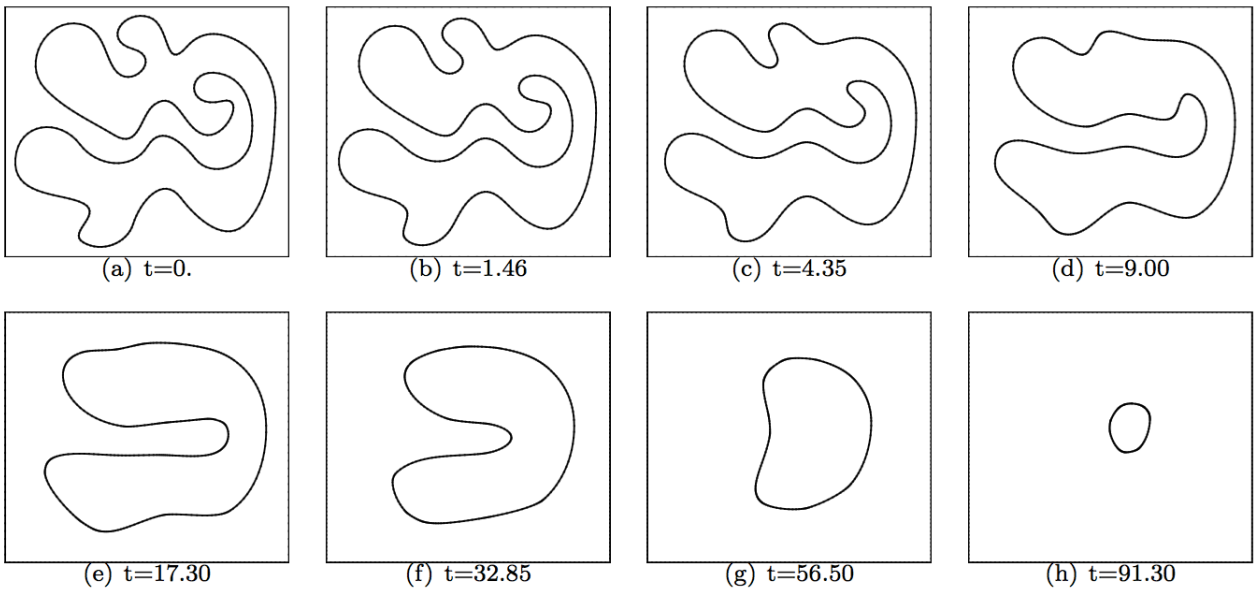

Figure 1.12: A smooth curve embedded in the plane evolves via curvature flow. The area bounded by the curve decreases at a constant rate, and the curve becomes progressively more circular; the curve eventually disappears in finite time, source: [17]

2

Different micro-structure models

A lot of different models have been developed to describe all the processes occurring in the micro-structure of steel. In this chapter the most prominent ones will be explained. Due to the fact that the current model is a Cellular Automata based model, the extension will have its basis formed by Cellular Automata. Interesting is to see that the different methods to calculate curvature-driven grain growth find their fundamental ideas in the micro-structure models described here.

2.1. Grain size distribution of Hillert

One of the earliest models to describe normal grain growth and the size distribution in the material was published by Hillert [20] in his paper in 1965 "On the theory of normal and abnormal grain growth". Now it is mostly used to verify the behaviour of new methods globally. He starts with equation (1.6) (Gibbs-Thompson)

$$v = M\Delta G = M\sigma(\frac{1}{R_x} + \frac{1}{R_y}). \tag{2.1}$$

Where M is the grain boundary mobility, γ the grain boundary energy and $R_{x,y}$ the principal radii of curvature. For this analysis the interest goes to the averaged value over all grains. To get the net increase of an averaged single grain a assumption has been made:

$$\frac{dR}{dt} = \alpha M\sigma(\frac{1}{R_{cr}} - \frac{1}{R}), \tag{2.2}$$

where R_{cr} is the critical size for which the grain either grows or shrinks and α a dimensionless constant. A steady state condition for the relative size $u = R/R_{cr}$ can be obtained from the equation (2.2). This is called the Lifshitz-Slyozov (LS) stability condition (see for a more detailed derivation the appendix of the article of Hillert):

$$\frac{du^2}{d\tau} = \gamma(u-1) - u^2, \text{ where } \tau = \ln R_{cr}^2 \text{ and } \gamma = 2\alpha M\sigma dt/dR_{cr}^2. \tag{2.3}$$

Next the Grain Size Distribution (GSD) is derived for both 2-D and 3-D case [20] and is given by:

$$P(u) = (2e)^{\beta}\frac{\beta u}{(2-u)^{2+\beta}}\exp\left(\frac{-2\beta}{2-u}\right). \tag{2.4}$$

Where $\beta = 2$ for the 2-D case and $\beta = 3$ for the 3-D case. Also the relative size u depends on the dimension, as shown in the appendix of Hillert the mean grain size is $\bar{R} = R_{cr}$ in the 2-D case and in the 3-D case $\bar{R} = 8/9R_{cr}$.

Remark: In constructing the Grain Size Distribution of Hillert, Neuman-Mullins relation[21] (explained in chapter 3) is used to determine the α in equation (2.2). As this relation was not available in 3-D at the time, simplifications have been made to estimate α. As will be introduced later, an exact relation in 3-D is found by R.D. MacPherson & D. J. Srolovitz [22]. Therefore improving the GSD for the 3-D case seems evident, as the distribution can be used to check whether the model works properly.

2.2. Level set Method

Together with the phase field method the level set method is used in a wide region of fields [23]. The basics of the level set method in the case of grain growth due to curvature is explained here. For a more in depth and general discussion see the work of Sethian and Osher [23].

The level set method gives a new view on how to describe a propagating interface. Rather than to follow the interface itself, the level set approach instead takes the original curve (left of figure 2.1) and builds it into a surface (right of figure 2.1). This cone shaped surface has a great property; it intersect the xy-plane exactly where the curve sits. This surface is called the level set function ϕ, a height function depending on the distance from the original curve. The original curve is called the zero level set, as it has zero height $\phi(\mathbf{x}(t), t) = 0$.

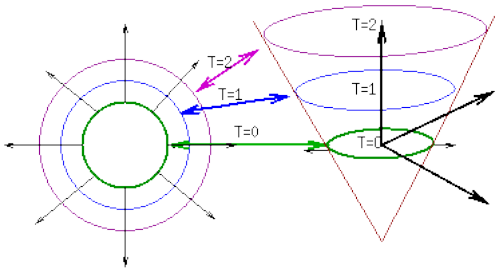

Figure 2.1: Left the original front lies in xy plane. Right the level set function, front is intersection of surface and xy plane. Here, T is the height function ϕ, source: [24]

Taking the total derivative of the level set function ϕ to t and with use of the chain rule we obtain:

$$\frac{\partial \phi}{\partial t}(\mathbf{x}, t) + \mathbf{x}_t(t)\frac{\partial \phi}{\partial \mathbf{x}}(\mathbf{x}, t) = 0, x \in \Omega \tag{2.5}$$

With the knowledge of equation (1.6) and the normal vector $\mathbf{N} = \frac{\nabla\phi}{|\nabla\phi|}$. The previous motion equation can be rewritten:

$$\phi_t + \nabla\phi\mathbf{x}_t = 0 \tag{2.6}$$

$$\phi_t + \nabla\phi C\kappa\mathbf{N} = 0 \tag{2.7}$$

$$\phi_t + C\kappa\nabla\phi\frac{\nabla\phi}{|\nabla\phi|} = 0 \tag{2.8}$$

$$\phi_t + C\kappa|\nabla\phi| = 0 \tag{2.9}$$

Now the growth of the interface is completely defined by the last equation.

2.3. Phase field

Here only the governing equations of the phase field method will be introduced. The main two ideas of the phase field a diffuse interface region (instead of a sharp one as used in the level set method) and the minimization over the free energy. Instead of a sharp interface the phase field function $\phi(x,t)$ of thickness ϵ is introduced which is a continuous function at the interface region. This function is for example given by:

$$\phi(x,0) = \begin{cases} 1 & \text{if x is in Grain A at time t,} \\ -1 & \text{if x is in Grain B at time t} \end{cases}$$

and at the the interface region characterized by $-1 < \phi(x,t) < 1$.

Now look at the function of the total free energy of a system:

$$\mathcal{F}(\phi,u) = \int_{\Omega} \left[f(\phi) + \epsilon^2 |\nabla\phi|^2 \right] d\Omega. \tag{2.10}$$

The function $f(\phi)$ gives the free energy of the system not effected by the boundary. The total free energy of the system depends heavily on the boundary and therefore the term $\epsilon^2|\nabla\phi|^2$ is added. The free-energy has to be minimized and the so called Euler-Lagrange equation is obtained. Thus minimize:

$$\frac{\delta\mathcal{F}}{\delta\phi} = 0. \tag{2.11}$$

A one dimensional example is given:

$$\frac{\partial f(\phi)}{\partial\phi} - 2\epsilon^2 \frac{d^2\phi}{dx^2} = 0. \tag{2.12}$$

The phase field method applied on the grain growth by curvature problem is found here [25].

2.4. Cellular Automata

Already in the 1940s at the currently called Los Alamos national laboratory the first hand was laid on what is called a Cellular Automata model. Here Stanislaw Ulam studied crystal growth. He represented the crystal surfaces as nodes in a lattice network and using one of the computers built for the Manhattan Project, he observed the changes to the surfaces as the nodes obeyed the rules that he imposed on them. He suggested a similar approach on a problem his colleague von Neumann was working on. Neumann listened and adopted the suggestion and called it Cellular Automata. Nowadays it is used for a great variety of applications e.g. computer processes, cryptography, biology etc.

A short description

A short description of a general CA model is given, for a more detailed work we refer to [26]. A n-dimensional subspace is divided in a finite number of volumes, called cells. All these cells have a state assigned to it, this can be any real number referring to the grain it belongs to. In the models described here the cell either belongs to an austenite or to a ferrite grain. The state of the cells depends on its neighbours and the state change rules defined. Whether a cell is neighbour cell of the cell considered depends on the neighbourhood definition. Most used definitions are Neumann (left), Moore (right) see figure 2.2. A state change rule defines the new state of a cell as a function of the states of all cells in the local neighbourhood of that cell. Note that due to the flexibility of the cellular automata lot of

different implementations exist!

Now a more mathematical description is given with the global state function Υ which is spatially partitioned into a finite number of cells. All cells i have a state ξ_i and a neighborhood η_i at discrete moments in time t_k, a state transformation function f_i^k is defined such that the new states can be computed depending on information solely from states and neighborhoods computed in previous time steps.

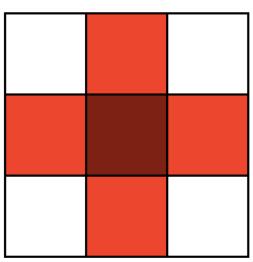

(a) Von Neumann neighbourhood

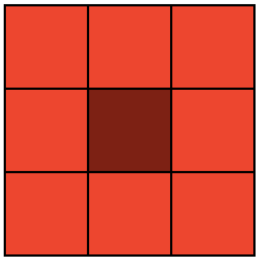

(b) Moore 3x3 neighbourhood

Figure 2.2: Two examples of most used neighbourhoods, source: [27]

Model by Bos et al.

In the article of Bos et al.[1] a description is given of the model developed for the metallurgical mechanisms occurring in the annealing stage of dual-phase steels. A summary is given here, where the focus lies on which metallurgical properties are included in the model and which are not.

In the CA-model the cells form grains which have the following properties:

- The phase of the grain
- Strain energy
- Average carbon concentration
- Carbon concentration at the interface

The growth of the grains is defined by the grain-boundary velocity v, determined by:

$$v = M\Delta G. \tag{2.13}$$

Here G depends on the grain and its properties. As an example we give the interface velocity for the ferrite growth in the austenitite to ferrite phase transformation:

$$v = M_0^{\alpha\gamma} exp(-Q_g^{\alpha\gamma}/RT)\Delta G_{\alpha\gamma}(x_C^{\gamma,int}), \tag{2.14}$$

where the following variables are denoted:

- $M_0^{\alpha\gamma}$, the pre-exponential factor for grain boundary mobility, the superscript denotes interface [m $J^{-1}s^{-1}$]
- $Q_g^{\alpha\gamma}$, Activation energy for the grain boundary mobility [kJmol^{-1}]
- R, the gas constant [J mol^{-1}K^{-1}]
- T, temperature in K

- $\Delta G_{\alpha\gamma}(x_C^{\gamma,int})$ [J mol^{-1}], the chemical driving force, where the variable $x_C^{\gamma,int}$ is the carbon concentration [weight %]

Recrystallization, transformation, nucleation and growth have already been included in the model, Mul [27] later changed the determination of the carbon interface concentration. Previously it was based on an exponential profile which was not accurate in the multi-grain model. The carbon concentration is now solved by using a finite difference grid on the austenite domain.

Still missing today is the growth due to surface tension or capillarity at the grain boundary. The impact of surface tension or capillarity is relatively small in the beginning of the process. When other forces stabilize the relative influence of curvature will continue to grow. This is the reason to further investigate this driving force and extent the current model available.

3

Methods to calculate curvature

This chapter first introduces the most intuitive method to calculate the curvature: the counting cell method. The principle of this method will only be introduced, as it is a very computationally costly method. Due to observations of Dunn and Chalmers [15, 16] the interests of this thesis will mainly go to vertex methods. One such method that has existed for some time is a method based on the minimization of grain boundary energy. A relatively new method has recently gotten more popular by the extension of the Neumann-Mullins relation in two dimensions in the recently published MacPherson-Srolovitz relation for three dimensions.

3.1. Counting cell method

The most intuitive method to calculate the curvature by counting cells is the one stated in Janssens [26]. In the case of a 2-D CA-model, template (see figure 3.1), in this case 5x5, is mapped over a cell at a grain boundary belonging to grain A. All cells not belonging to grain A are assigned state $\phi_k = 0$. All the cells belonging to grain B are labeled by $\phi_k = 1$. The sum over all these cells (in this case $n = 25$) gives a value that can be scaled to a certain curvature. An example of this scaling is given below, where ϕ represents the state of the cell and ϵ a certain scaling, results in the following curvature:

$$\kappa = 15 - \sum_{k=1}^{n} \phi_k \epsilon_k. \tag{3.1}$$

Another way of obtaining this number is by using the following equation from Nastac's model[28]. This idea comes from the cellular automata solidification model where curvature also plays an important role.

$$\kappa(A) = \frac{1}{\Delta x}(1 - 2\frac{f_s + \sum_{i=1}^{n} f_s(i)}{n+1}), \tag{3.2}$$

where $f_s(i)$ represents the solid fraction of the cell (solid cell $f_s(i) = 1$, liquid cell $f_s(i) = 0$, interface cell $0 < f_s < 1$) and Δx the grid size. A more accurate method is the so called Variation of Unit Vector Normal (VUVN) [28] and is described as follows:

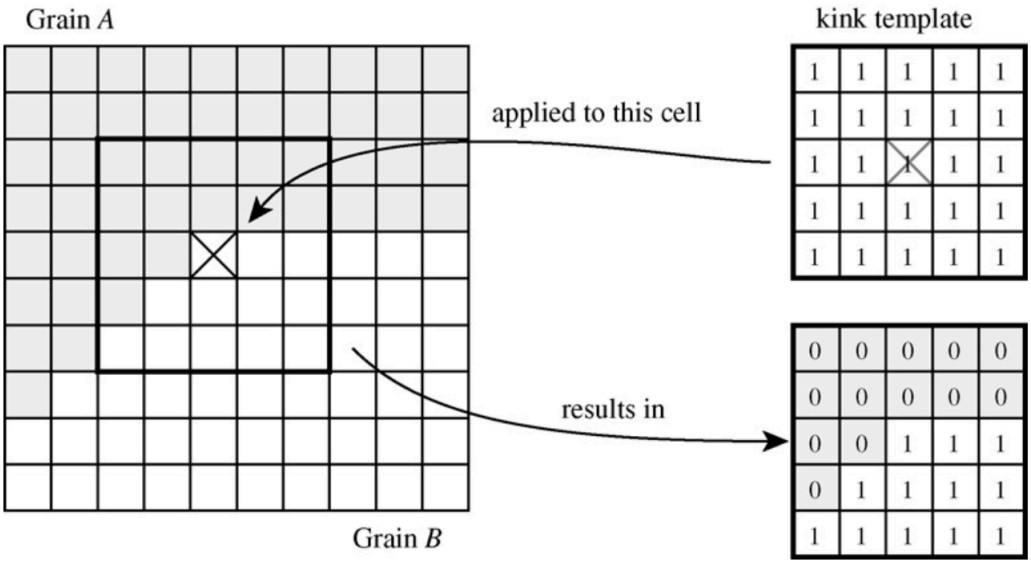

Figure 3.1: Counting cell method where a 5x5 template is mapped over the cell where the curvature is calculated from, source [26]

$$\kappa = \frac{2\frac{\partial f_s}{\partial x}\frac{\partial f_s}{\partial y}\frac{\partial^2 f_s}{\partial x \partial y} - (\frac{\partial f_s}{\partial y})^2\frac{\partial^2 f_s}{\partial x^2} - \frac{\partial^2 f_s}{\partial y^2}}{\left[(\frac{\partial f_s}{\partial x})^2 + (\frac{\partial f_s}{\partial y})^2\right]^{\frac{3}{2}}}. \tag{3.3}$$

This is an analytical method and as the CA model is a sharp interface model, finite difference is difficult to apply, therefore bilinear interpolation is used, see figure 3.2. The curvature corresponding to the cell in the center of the 5x5 template mapped over this cell, this is f_{13}. We use f_i (i=1-25) the solid fraction of each cell and F_i the linearly interpolated variable by the average of four neighbour cells (for example: $F_1 = \frac{1}{4}(f_2 + f_3 + f_7 + f_8)$). The following computations are needed:

$$\bar{f_8} = \frac{1}{4}(F_1 + F_2 + F_4 + F_5), \tag{3.4}$$

$$\bar{f_{12}} = \frac{1}{4}(F_3 + F_4 + F_7 + F_8), \tag{3.5}$$

$$\bar{f_{14}} = \frac{1}{4}(F_5 + F_6 + F_9 + F_10), \tag{3.6}$$

$$\bar{f_{18}} = \frac{1}{4}(F_8 + F_9 + F_11 + F_12), \tag{3.7}$$

$$\frac{\partial f_{13}}{\partial x} = (\bar{f_{14}} - \bar{f_{12}})/(2\Delta x), \tag{3.8}$$

$$\frac{\partial f_{13}}{\partial y} = (\bar{f_8} - \bar{f_{18}})/(2\Delta x), \tag{3.9}$$

$$\frac{\partial^2 f_{13}}{\partial x \partial y} = (F_4 + F_9 - F_5 - F_8)/(\Delta x)^2, \tag{3.10}$$

$$\frac{\partial^2 f_{13}}{\partial x^2} = (\bar{f_{14}} + \bar{f_{12}} - 2\bar{f_{13}})/(\Delta x)^2, \tag{3.11}$$

$$\frac{\partial^2 f_{13}}{\partial y^2} = (\bar{f_8} + \bar{f_{18}} - 2\bar{f_{13}})/(\Delta x)^2. \tag{3.12}$$

Hence, a lot of computational power is needed to calculate the curvature via this method, though a higher accuracy is reached. From Wei[28] it is given that a 2-D simulation takes within 2 hours and a

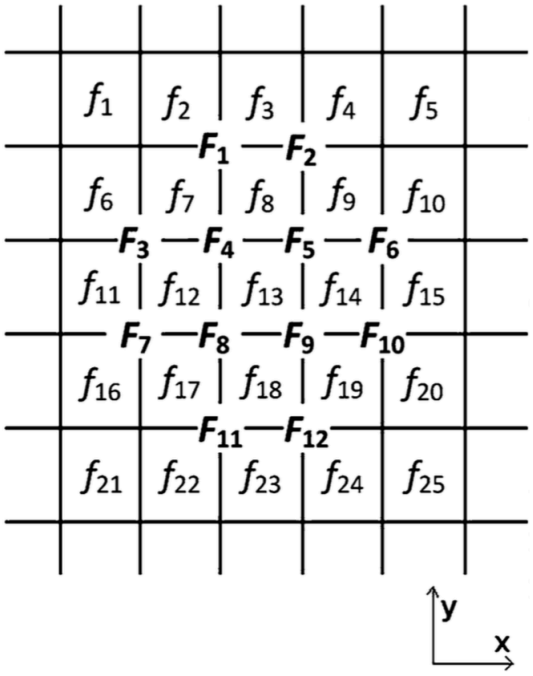

Figure 3.2: Bilinear interpolation of a 5x5 template, source: [29]

3-D simulation within 24 hours. Other alternative methods have been introduced: Convolved Volume of Fluid (VOF), Reconstructed Distance Function, Height Function.

3.1.1. VUVN and their different methods

The three techniques are compared in [30]. First they will be shortly introduced and then the results of the convergence and error analysis will be given.

Convolved VOF technique

Here the VOF function is convolved with a smoothing kernel, this is needed to even more smoothing the interface. A convolved function is calculated with:

$$\bar{f}_a = \int f_b K\left(\frac{|\mathbf{r}_a - \mathbf{r}_b|}{h}\right) dV_b. \tag{3.13}$$

Here K is the convolution kernel see [31] for more detail. Then the following equation for the curvature can be used:

$$\kappa = -\nabla\left(\frac{\nabla \bar{f}}{|\nabla \bar{f}|}\right) = \frac{\bar{f}_{xx} n_y^2 + \bar{f}_{yy} n_x^2 - 2 n_x n_y \bar{f}_{xy}}{\left(n_x^2 + n_y^2\right)^{\frac{3}{2}}}, \tag{3.14}$$

where $\mathbf{n} = (n_x, n_y) = (\frac{\partial \bar{f}}{\partial x}, \frac{\partial \bar{f}}{\partial y})$, and standard finite difference used on all derivatives in the function.

Reconstructed Distance Function (RDF)

The curvature is calculated with the RDF technique by:

$$\kappa = -\nabla\left(\frac{\nabla \phi}{|\nabla \phi|}\right) = \frac{\phi_{xx} n_y^2 + \phi_{yy} n_x^2 - 2 n_x n_y \phi_{xy}}{\left(n_x^2 + n_y^2\right)^{\frac{3}{2}}}, \tag{3.15}$$

where ϕ is the RDF, how to calculate the RDF can be found in [30] and $\mathbf{n} = (n_x, n_y) = (\frac{\partial \phi}{\partial x}, \frac{\partial \phi}{\partial y})$. All other derivatives are calculated using finite difference.

Height function

The technique is defined as follows:

1. find the direction of the maximal normal in orde to orient the height function
2. sum the volume fractions to evaluate locally the height function $X(y)$ or $Y(x)$
3. compute the curvature by differentiating the height function only if the height function lies within the cell dimensions

Conclusion

We see in the error analysis given by [30] that there is no clear answer to which method performs best. One suggestion is made that the HF method is best used when κh is small (below $\frac{1}{5}$), otherwise use either CV or RDF. Notice that this means that $h \leq \frac{1}{5\kappa}$ and hence h should be small for large κ.

3.2. Vertex methods

From the observation of Dunn[16], Chalmers[15], that the effects of curvature near the edges of a grain are more pronounced than in the center of grain faces, three methods are introduced who take the vertex as the starting point from which surface tension driven grain growth is modelled. The first method by Nippon, uses the grain boundary energy belonging to each particular grain to force the position of the vertices in an equilibrium state. The second method minimizes the grain boundary energy to obtain the equation of motion. The third method uses the exact solution of the total area of grain growth, with help of the Neumann-Mullins relation [21].

3.2.1. Vertex by Nippon

Mathematically the most basic method is given here. Key here is the need of the correct grain boundary energy γ per grain boundary edge. Therefore only the governing equations and a short discussion of the method by Tamaki [32] will be given.

$$\mathbf{v}_{gb,i} = M_{gb,i}\gamma_i\kappa_i \tag{3.16}$$

$$\mathbf{v}_{triple,i} = M_{triple,i}\sum_{j=1}^{3}\gamma_{ij}\frac{\mathbf{r}_{ij}}{|\mathbf{r}_{ij}|} \tag{3.17}$$

In figure 3.3 the method is illustrated. To obtain the curvature κ, a formula is used which calculates the radius of a circumscribed circle around three virtual vertices. Notice: that the equilibrium angles at the triple are not forced in this method as is done in the methods that will be discussed afterwards.

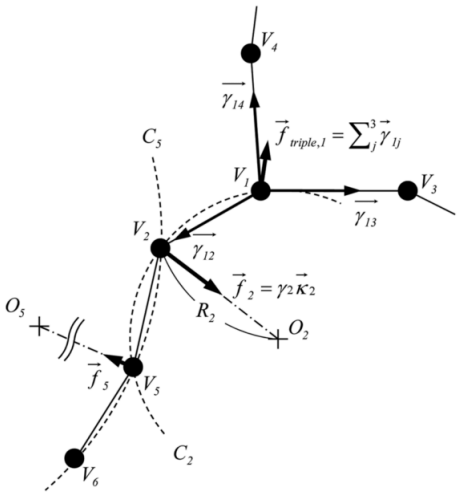

Figure 3.3: Local curvature multi-vertex model, source: [32]

3.2.2. Minimization of grain boundary energy

An approach based on minimization of grain boundary energy has been proposed by Fullmann[33] in 1952. Recent developments based on Fullmann are so called vertex models. It gives the possibility to treat the influence of both the energy and the mobility of grain-boundaries. Fundamental to the vertex model is the coupling of the dissipative energy and the potential energy. The dissipative equation of motion is presented by the potential function $\mathcal{F}\{q\}$ and the Rayleigh dissipation function $\mathcal{R}(\{\dot{q}\},\{q\})$ where $\{q\} = q_1, q_2, \ldots$ are a discrete set of dynamical variables. Hence,

$$\frac{\partial \mathcal{F}}{\partial q_i} = -\frac{\partial \mathcal{R}}{\partial \dot{q}}. \tag{3.18}$$

This expresses the relation between the frictional force on the left and the static force on the right. To find the equations of motion for the vertices a minimization problem has to be solved to obtain the Euler-Lagrange equation.

Euler-Lagrange

In this section we will derive the Euler-Lagrange equation [34] for the dissipation function and potential. Next with calculus of variation the first the Euler-Lagrange equation is derived. Later the dissipative term is added to obtain the relation:

$$\frac{\partial \mathcal{R}}{\partial \dot{q}_i} = -\frac{\partial \mathcal{F}}{\partial q_i} \tag{3.19}$$

First consider the minimization problem:

$$\min_q F(q) = \min_q \int_{t_0}^{t_1} \mathcal{L}(t, q, \nabla q) dt, \tag{3.20}$$

with boundary condition $q(t_0) = t_0$, sufficiently smooth function F and let there exist a minimum $F(\hat{q})$. When searching for the minimum $F(\hat{q})$ the following must hold:

$$F(\hat{q}) \leq F(\hat{q} + sv) \qquad \forall v \in \mathbb{R}. \tag{3.21}$$

Let $\Psi(s) = F(\hat{q} + sv)$, then for $\hat{q}$ to be the minimum, it holds $\Psi(0) \leq \Psi(s)$, with s an arbitrary parameter. Using Fermat's theorem:

$$0 = \Psi'(0) \tag{3.22}$$

$$= \frac{d}{ds} F(\hat{q} + sv)|_{s=0}. \tag{3.23}$$

Using variations we take $q(t) = \hat{q}(t) + sv(t)$, a family of curves around the solution $\hat{q}(t)$ and $v(t)$ an arbitrary sufficiently smooth curve satisfying $v(t_0) = 0$ from the boundary condition. Substitution gives:

$$F(q) = \int_{t_0}^{t_1} \mathcal{L}(t, \hat{q} + sv(t), \nabla(\hat{q} + sv(t)) dt. \tag{3.24}$$

The integral over the function where $\hat{q}$ is a given solution is a function of s denoted by $\Psi(s)$. $\Psi(s)$ is minimal for $q = \hat{q}$, hence $s = 0$. The following relation has to hold for the existence of a minimum in $s = 0$

$$\left.\frac{dF(\hat{q}+sv)}{ds}\right|_{s=0} = 0, \tag{3.25}$$

$$\int_{t_0}^{t_1}\left[\frac{\partial \mathcal{L}}{\partial q}(t,\hat{q},\nabla\hat{q})v(t) + \frac{\partial \mathcal{L}}{\partial \frac{\partial q}{\partial t}}(t,\hat{q},\nabla\hat{q})\frac{\partial v}{\partial t}\right]dt = 0, \tag{3.26}$$

$$\int_{t_0}^{t_1}\left[\frac{\partial \mathcal{L}}{\partial q} - \frac{d}{dt}\frac{\partial \mathcal{L}}{\partial \dot{q}}\right]v(t)dt + \left[v(t)\frac{\partial \mathcal{L}}{\partial \dot{q}}\right]_{t_0}^{t_1} = 0. \tag{3.27}$$

Both parts of equation 3.27 have to equal zero. Let us take $v(t_1) = 0$ and as $v(t_0) = 0$, then with the lemma of Dubois-Reymond, the minimization problem is solved if:

$$\frac{\partial \mathcal{L}}{\partial q} - \frac{d}{dt}\frac{\partial \mathcal{L}}{\partial \dot{q}} = 0. \tag{3.28}$$

Now we allow dissipation in the system, therefore the Lagrangian is slightly changed. The result follows from the D'Alembert principle dissipation is added allow friction.

$$\frac{\partial \mathcal{L}}{\partial q} - \frac{d}{dt}\frac{\partial \mathcal{L}}{\partial \dot{q}} = -\frac{\partial \mathcal{R}}{\partial \dot{q}_i}$$

When the Lagrangian is only a function of the potential this gives the required equation,

$$\frac{\partial \mathcal{F}}{\partial q_i} + 0 = -\frac{\partial \mathcal{R}}{\partial \dot{q}_i} \tag{3.29}$$

$$\frac{\partial \mathcal{F}}{\partial q_i} = -\frac{\partial \mathcal{R}}{\partial \dot{q}_i} \tag{3.30}$$

Discretizing the dissipation and potential function

Here first an expression for both the potential term of the total energy and the dissipative term is given. Then this will be discretized such that we can use it later in the implementation of the given method [35–37]. We have the following two expressions for the grain boundary energy:

$$\mathcal{F}(\{\mathbf{r}\}) = \int_{\Gamma_{grain}} \sigma(a)da \tag{3.31}$$

$$\mathcal{R}(\{\mathbf{r}\},\{\dot{\mathbf{r}}\}) = \frac{1}{2}\int_{\Gamma_{grain}} \frac{v(a)^2}{m_{GB}(a)}da \tag{3.32}$$

In the above relations, we have:

- Γ_{grain} is the boundary of a grain
- $\gamma(a)$ is the grain-boundary energy at the given position a
- $v(a)$ is the normal velocity of the grain boundary
- m_{GB} is the grain-boundary mobility at position a, usually this function is constant over the interface between two grains

The integrals will be transformed into a sum of integrals over segments. A segment in $\mathbb{R}^2$ is defined by the straight line connecting two vertices with positions $\mathbf{r}_i$ and $\mathbf{r}_j$. Also the grain-boundary energy and mobility are now defined per segment ij. Define $\mathbf{r_{ij}} = \mathbf{r}_i - \mathbf{r}_j$. Which gives:

$$\mathcal{F}_{<ij>} = \int_{<ij>} \sigma(r)dr = \sigma \mathbf{r}_{ij} = \sigma|\mathbf{r}_i - \mathbf{r}_j|, \tag{3.33}$$

$$\mathcal{R}_{<ij>} = \frac{1}{2m_{ij}} \int_{<ij>} v(a)^2 da. \tag{3.34}$$

Define the normal vector of each segment as,

$$\mathbf{n}_{ij} = \frac{1}{||\mathbf{r}_{ij}||} \begin{bmatrix} -y_{ij} \\ x_{ij} \end{bmatrix}. \tag{3.35}$$

To obtain the $v(a)$ use the known position $a \in < ij >$ and take the weighed average of the influence of both velocities of the vertex i and j. Hence the normal component of the velocity reads,

$$v(a) = \frac{1}{|\mathbf{r}_{ij}|}(|\mathbf{r}_{aj}|\mathbf{v}_i + |\mathbf{r}_{ai}|\mathbf{v}_j) \bullet \mathbf{n}_{<ij>}. \tag{3.36}$$

Substitution gives:

$$\mathcal{R}_{<ij>} = \frac{1}{6}\frac{||\mathbf{r}_{ij}||}{m_{ij}} \left[(\mathbf{v}_i \bullet \mathbf{n}_{<ij>})^2 + (\mathbf{v}_j \bullet \mathbf{n}_{<ij>})^2 + (\mathbf{v}_i \bullet \mathbf{n}_{<ij>})(\mathbf{v}_j \bullet \mathbf{n}_{<ij>})\right]. \tag{3.37}$$

Summing over all connected pairs $< ij >$ (where $\sum_j^{(i)}$ denotes the sum over j connected to i),

$$\mathcal{F}\left(\{\mathbf{r}\}\right) = \frac{1}{2}\sum_{i=1}^{N}\sum_{j}^{(i)} \sigma_{ij}||\mathbf{r}_{ij}||, \tag{3.38}$$

$$\mathcal{R}(\{\mathbf{r}\},\{\dot{\mathbf{r}}\}) = \frac{1}{6}\sum_{i=1}^{N}\sum_{j}^{(i)} \frac{||\mathbf{r}_{ij}||}{m_{ij}} \left[(\mathbf{v}_i \bullet \mathbf{n}_{<ij>})^2 + (\mathbf{v}_j \bullet \mathbf{n}_{<ij>})^2 + (\mathbf{v}_i \bullet \mathbf{n}_{<ij>})(\mathbf{v}_j \bullet \mathbf{n}_{<ij>})\right]. \tag{3.39}$$

When substituting in the Lagrange function we get:

$$\frac{1}{3m_{ij}}\sum_{j}^{(i)} |\mathbf{r}_{ij}|\mathbf{n}_{<ij>}\mathbf{n}_{<ij>} \bullet (\mathbf{v}_i - \frac{1}{2}\mathbf{v}_j) = -\sum_{j}^{(i)} \frac{\mathbf{r}_{ij}}{|\mathbf{r}_{ij}|}. \tag{3.40}$$

We can write this equation into the following system

$$\mathcal{D}_i \mathbf{v}_i = \mathbf{f}_i - \frac{1}{2} \sum_j^{(i)} \mathcal{D}_{ij} \mathbf{v}_j, i = 1...N \tag{3.41}$$

$$\mathcal{D}_{ij} = \frac{1}{3m_{ij}||\mathbf{r}_{ij}||} \begin{bmatrix} y_{ij}^2 & -x_{ij}y_{ij} \\ -x_{ij}y_{ij} & x_{ij}^2 \end{bmatrix}, \tag{3.42}$$

$$\mathcal{D}_i = \sum_j^{(i)} \mathcal{D}_i, \tag{3.43}$$

$$\mathbf{f}_i = \frac{\partial \mathcal{F}}{\partial \mathbf{r}_i} = -\sum_j^{(i)} \sigma_{ij} \frac{\mathbf{r}_{ij}}{||\mathbf{r}_{ij}||}. \tag{3.44}$$

In Kawasaki the system of equations is further simplified. This will not be done as the convergence to equilibrium state is not happening because of the simplification according to D. Weygand [35].

3.2.3. Vertex method using Neumann-Mullins equation

In 2009 the article "A more accurate two-dimensional grain growth algorithm" has been published by Lazar, MacPherson and Srolovitz [38]. Here the Neumann-Mullins relation [21] (an exact relation for grain growth in two dimensions using the number of vertices) is used to obtain a method describing the grain growth due to surface tension. Although a two-dimensional algorithm is in theoretical perspective usefull in practice, as micro-structures are three dimensional and as up to 2007 there was no extension of the Neumann-Mullins relation to three or higher dimensions, it was not. This changed in 2007 when Robert D. MacPherson together with David J. Srolovitz published the article "The von Neumann relation generalized to coarsening of three-dimensional microstructures" in Nature [22]. For now only the two dimensional case is considered, but extending to three dimensions seems evident [39].

First the proof of Neumann-Mullins relation will be discussed. Then the results of [21] will be used to obtain a method for grain growth in two dimensions, as proposed in [38].

Deriviation of Neumann-Mullins equation

In 1956 Mullins published the article called: "Two dimensional motion of idealized grain boundaries" [21]. Here he proofed a general theorem concerning the change of area enclosed by a curve in two dimensions. This curve is defined as $r(\theta,t)$, where r and θ are polar coordinates and t time. Assumed is that any point of the curve moves towards it center of curvature with a velocity v, given by $v = M\gamma\kappa$, where M is the grain boundary mobility and γ the grain boundary energy. Define the arc length s of a curve α as $s(\alpha) = \int_a^b |\alpha'(t)|dt$. From figure 3.4 it can be seen that $\Delta r \sin\psi = -M\gamma\kappa\Delta t$. Using the relations $\kappa = \frac{\partial\beta}{\partial s}$ and $\sin\psi = r(\frac{\partial\theta}{\partial s})$ a new relation for $\frac{\partial r}{\partial t}$ can be obtained:

$$\frac{\partial r}{\partial t} = -M\gamma\frac{\kappa}{\sin\psi} = -M\gamma\frac{1}{r}\frac{\partial\beta}{\partial\theta}. \tag{3.45}$$

The area enclosed by a simple closed curve is given by $A = \frac{1}{2}\oint_0^{2\pi} r^2 d\theta$, where the integral is taken counterclockwise around the curve.

Using these two results and differentiating over time gives:

$$\frac{dA}{dt} = \oint \frac{\partial r}{\partial t} r d\theta = -M\gamma \oint \frac{\partial\beta}{\partial\theta} d\theta = -M\gamma \oint d\beta = -2\pi M\gamma. \tag{3.46}$$

Remark: the result also holds for M,γ being a function of β.

From this relation it can be concluded that two curves of different shape, but enclosing equal areas have an equal growth rate!

Now a similar relation will be obtained for a two dimensional area of grain boundaries. A network of arbitrary curves dividing the plane into polygon-like grains is presented, see figure 3.5. As an illustration a grain with n sides is considered, the vertices are numbered counter clockwise, each side has the same number corresponding to the preceding vertice. Let β_{ij} be the angle between the x-axis and the tangent to i-th side and through the j-th vertex. The angle between each edge is assumed to be $\frac{2\pi}{3}$ or 120 degrees, as explained in Chapter one. Though when γ is dependent on the grains it belongs to (anisiotropic), a different equilibrium angle can be derived. Using the relation of equation (3.46), we find the rate of change of area of the grain to be:

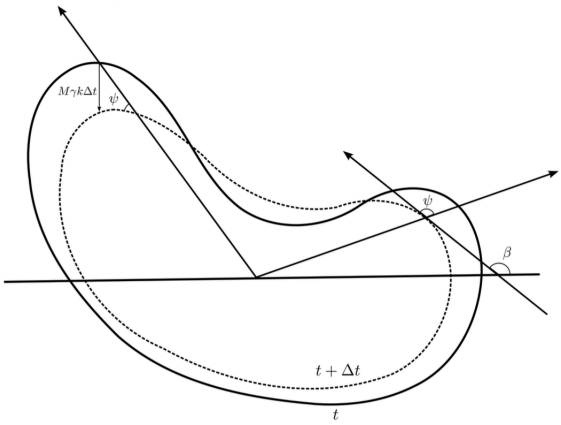

Figure 3.4: Closed curve which moves towards it center of curvature, source: [21]

$$\frac{dA}{dt} = -M\gamma \oint d\beta, \tag{3.47}$$

$$= -M\gamma \left[(\beta_{11} - \beta_{12}) + (\beta_{22} - \beta_{23}) + (\beta_{33} - \beta_{34}) + \ldots + (\beta_{nn} - \beta_{n1})\right], \tag{3.48}$$

$$= -M\gamma \left[(\beta_{22} - \beta_{12}) + (\beta_{33} - \beta_{23}) + \ldots + (\beta_{11} - \beta_{n1})\right]. \tag{3.49}$$

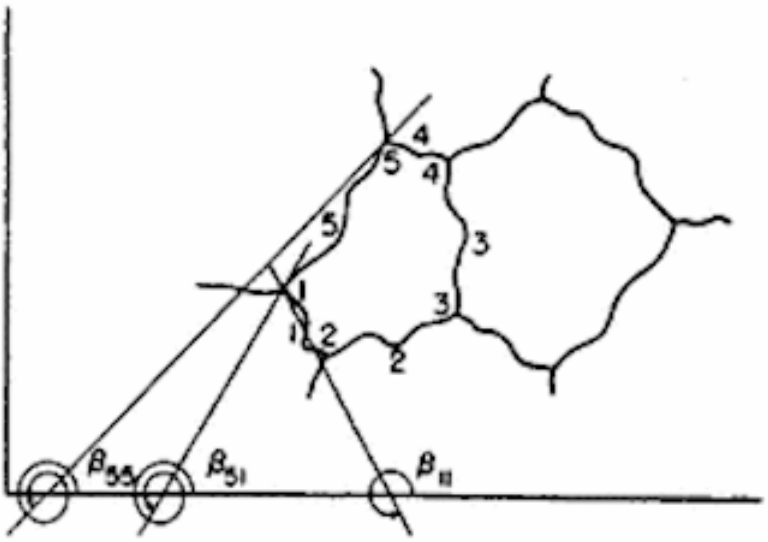

Figure 3.5: Two dimensional area of grain boundaries, source: [21]

From figure 3.6 it can be concluded that $\beta_{22} - \beta_{12} = \pi - \frac{2\pi}{3} = \frac{\pi}{3}$ which is the case for the first $n-1$ terms. From figure 3.5 $\beta_{11} - \beta_{51} = \frac{\pi}{3} - 2\pi$. Hence,

$$\frac{dA}{dt} = -M\gamma \left[(n-1)\frac{\pi}{3} - 2\pi + \frac{\pi}{3}\right] = -M\gamma \frac{\pi}{3}(6-n). \tag{3.50}$$

Implementation of Neumann-Mullins relation in vertex method by Lazar et al. [38]

The following idea is considered: use the knowledge of the total grain growth (Neumann-Mullins relation, which is the exact for normal grain growth in an isotropic polycrystal) of one particular grain and

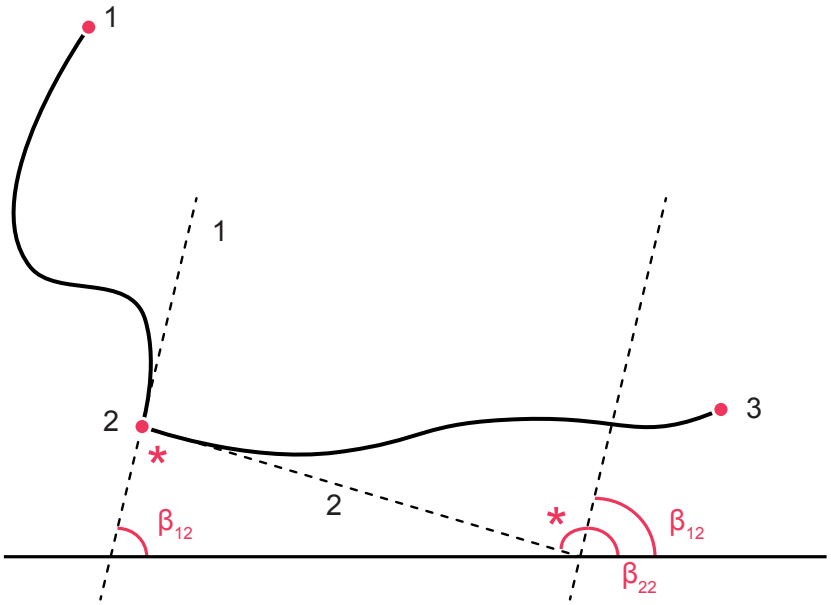

Figure 3.6: A closer look on how the β is constructed

divide this growth over all the vertices.

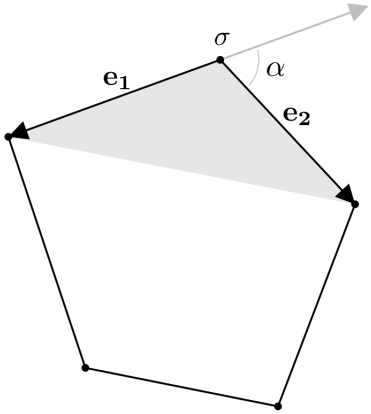

Figure 3.7: Single grain, node σ with displacement vector and edges $\mathbf{e}_1$,$\mathbf{e}_2$ connected to σ, source: [38]

For simplicity first a single isolated grain is considered see figure 3.7, hence $n = 0$. A key observation is that when changing the area locally the total area is changed with the same amount. When for example the position of the vertex$\boldsymbol{\sigma}$ is changed, only the gray area is affected and the total area of the grain changes with the same amount. Therefore when using the derived relation above (3.50) and by summing over over all nodes separately:

$$\Delta A = 2\pi M\gamma(\frac{0}{6} - 1)\Delta t = -2\pi M\gamma\Delta t \tag{3.51}$$

$$= \sum_{i=1}^{n} -\alpha_i M\gamma\Delta t, \text{ where } \sum_{i=1}^{n} \alpha_i = 2\pi. \tag{3.52}$$

First the equation of motion of a virtual vertex is derived. This is a vertex which has only two neighbouring grains and therefore only has two neighbouring vertices. Make use of the fact that $n = 0$ for a virtual vertex and a local change in area by moving a vertex is exactly the same as the global change in area. Consider a node $\boldsymbol{\sigma}$ with edges $\mathbf{e_1}$ and $\mathbf{e_2}$ as shown in Figure 3.7. The exterior angle α_i, from the cosine law $\alpha_i = \cos^{-1}\left(-\frac{\mathbf{e_1}\mathbf{e_2}}{|\mathbf{e_1}||\mathbf{e_2}|}\right)$. Node $\boldsymbol{\sigma}$ is moved by a displacement vector $\mathbf{v}_i$ belonging to vertex i, which will change the area of the triangle by $\Delta A = -\alpha_i M\gamma\Delta t$ (using equation 3.51. For numerical stability reasons node σ is moved in the direction of $\mathbf{e_1} + \mathbf{e_2}$. Hence,

$$\mathbf{v}_i = \alpha_i M\gamma\Delta t \frac{\mathbf{e_1} + \mathbf{e_2}}{|\mathbf{e_1} \times \mathbf{e_2}|}. \tag{3.53}$$

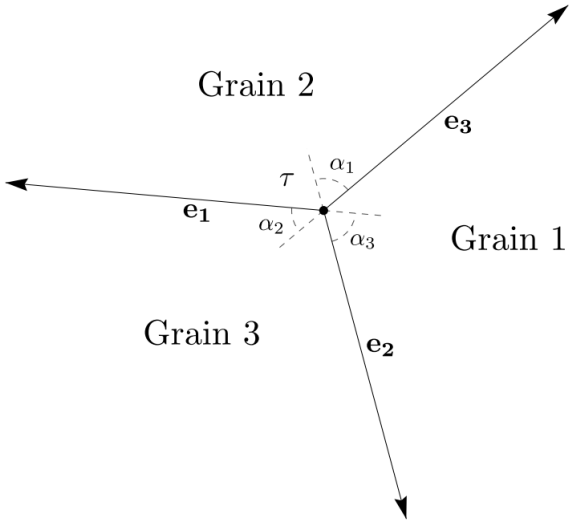

Figure 3.8: Triple defined by its vectors belonging to the edges connected to the triple and exterior angles α_{ji}, source: [38]

Now considered will be a triple junction node $\boldsymbol{\tau}$ (or node i in general) as shown in figure 3.8. Again the Neumann-Mullins relation is considered, now for the displacement of the triple junction node. Because there are three different grains meeting at a triple point the relation $\Delta A_j = -(\alpha_j - \frac{\pi}{3})M\gamma\Delta t$ holds, where α_{ji} is the exterior angle at the triple junction with respect to grain j. When one grain has n triples this means it also has exactly n neighbouring grains. Therefore,

$$\sum_{i=1}^{n}(\alpha_{j,i} - \frac{\pi}{3})M\gamma\Delta t = (2\pi - \frac{n\pi}{3})M\gamma\Delta t, \tag{3.54}$$

$$= -2\pi M\gamma(1 - \frac{n}{6}). \tag{3.55}$$

The α's are given by:

$$\alpha_{1,i} = \cos^{-1}\left(-\frac{\mathbf{e_{1,i}}\mathbf{e_{2,i}}}{|\mathbf{e_{1,i}}||\mathbf{e_{2,i}}|}\right), \tag{3.56}$$

$$\alpha_{2,i} = \cos^{-1}\left(-\frac{\mathbf{e_{2,i}}\mathbf{e_{3,i}}}{|\mathbf{e_{2,i}}||\mathbf{e_{3,i}}|}\right), \tag{3.57}$$

$$\alpha_{3,i} = \cos^{-1}\left(-\frac{\mathbf{e_{3,i}}\mathbf{e_{1,i}}}{|\mathbf{e_{3,i}}||\mathbf{e_{1,i}}|}\right). \tag{3.58}$$

The following system of equations need to be solved:

$$\begin{bmatrix} \mathbf{e_{1,i}} - \mathbf{e_{2,i}} \\ \mathbf{e_{2,i}} - \mathbf{e_{3,i}} \\ \mathbf{e_{3,i}} - \mathbf{e_{1,i}} \end{bmatrix} \mathbf{v}_i = 2M\gamma\Delta t \begin{bmatrix} \alpha_{1,i} - \frac{\pi}{3} \\ \alpha_{2,i} - \frac{\pi}{3} \\ \alpha_{3,i} - \frac{\pi}{3} \end{bmatrix}. \tag{3.59}$$

Due to the fact that there are three equations and the degree of freedom is two. The number of equations can be reduced, obtain:

$$\mathbf{v}_i = 2M\gamma\Delta t \begin{bmatrix} 0 & -1 \\ 1 & 0 \end{bmatrix} \begin{bmatrix} \mathbf{e_{1,i}} - \mathbf{e_{2,i}} \\ \mathbf{e_{2,i}} - \mathbf{e_{3,i}} \end{bmatrix}^{-1} \begin{bmatrix} \alpha_{1,i} - \frac{\pi}{3} \\ \alpha_{2,i} - \frac{\pi}{3} \end{bmatrix}. \tag{3.60}$$

4

Implementation

In the end the cellular automata model needs to expended by a curvature-driven grain growth method. The idea is to extract the vertices from the cellular automata model. The result of the model is very similar to a voronoi, and to get a preliminary result a simple voronoi has to be made. From [35] vertices are needed to allow a finer grid and therefore a better solution. Some additional rules need to be forced, so called 'topological transformations'. Finally some test cases will be introduced which will be needed in order to verify the implementation and to make a well reasoned decision on which method is best suited.

4.1. Virtual vertex & Topological transformations

In the original paper of Kawasaki [37] where the first two dimensional vertex model was proposed, only triple points were used. Further development in three dimensions revealed that more information of the edges is required. Therefore, a second kind of vertex is introduced: the virtual vertex [35]. These new introduced vertices are placed between a pair of triple points (called 'real vertices'), to allow a more finer grid over the edges.

Define $n_{virtual}$ as the number of virtual vertices between two triple points, the precision of the discretization and therefore the precision of the approximation of the curvature depends on this number. A second parameter needs to be introduced, the minimal distance between two virtual vertices for which otherwise one vertex needs to be removed. Due to grain growth the structure will change, hence the number of virtual vertices need to depend on the mean grain size $< r >$. Therefore, the minimum distance, Δ between virtual vertices is given [37]:

$$\Delta = \frac{\alpha}{n_{virtual} + 1} < r >, \tag{4.1}$$

where $< r >= [(2A_{total})/(\pi n_{real})]^{\frac{1}{2}}$ using Eulers relation in two dimensions, A_{total} the size of the system, n_{real} the number of triple points in the system. The pre-factor α is chosen small enough (0.025 in Weygand et al. [35]) to have negligible influence on the size distribution of the grains. When the distance between two real vertices is larger than $2.5 n_{virtual}\Delta$, $n_{virtual}$ virtual vertices are introduced.

When triple points become too close, a number of topological transformations needs to be enforced. We identify three transformations, the first two between real vertices, the last because of the introduction of virtual vertices.

1. Recombination of triple points
2. Annihilation of three sided grains of a small area
3. Disappearance of a grain created out of two virtual vertices (though happens rarely)

The first topological transformation (seen in figure 4.1a) removes a triple point when the distance between two triples become smaller than Δ. Two triple points are so close to each other such that they form a point where four grains meet. Because of instability of such a points, the point splits again and forms two triples. The second topological transformation (seen in figure 4.1b) removes two triple point when a three sided grain which has one side smaller than Δ and the other sides smaller than 2Δ. In this case the size of the grain is smaller than Δ^2. The third transformation (seen in figure 4.1c) removes a grain when it is formed of two real vertices.

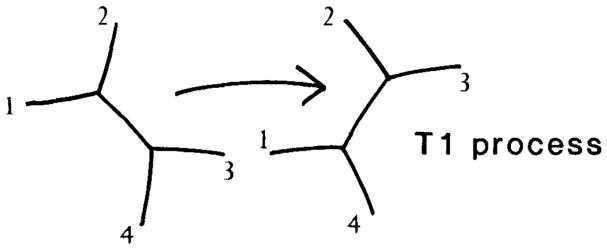

(a) Transformation 1

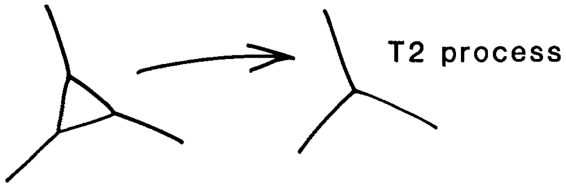

(b) Transformation 2

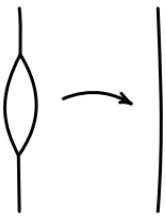

(c) Transformation 3

Figure 4.1: Topological transformations, source: [35]

4.2. Testing

From theory three methods have been selected to investigate further. To compare the methods a number of test cases have been constructed. Distinguish two ways of testing whether the method works appropriately. First the most important one, the methods are compared with the analytic solution. Here the vertices are placed on a circle because the exact curvature of a circle and thus a comparison is with the exact solution is possible. The second test is comparing the found solution with an analytical implementation of the method on the selected test case. This has been done by substituting an analytical representation of the problem in the method [35].

Simple polygon

First a polygon where the vertices lay on a circle is constructed. Knowing the exact curvature of a circle, the displacement of a vertex using different methods can be compared with the displacement according to the Gibbs-Thompson effect: $v = -M\gamma\kappa$.

Another way is introduced by Weygand et al. [35], he makes use of equation (3.41) to find the analytic solution of the change in total area of a n-sided polygon. See appendix A to see the derivation which leads to:

$$\frac{dA'_n}{dt} = -2M\gamma n \tan(\frac{\pi}{n}). \tag{4.2}$$

By taken the limit of $n \to \infty$ it can be seen that it is similar to the exact solution of a circle:

$$\lim_{n\to\infty} \frac{dA'_n}{dt} = -2\pi M\gamma, \tag{4.3}$$

which is the Neumann-Mullins relation for $n = 0$. Note: Here the dissipation and potential term is used as a starting point, which of course is already an approximation of the influence of the surface tension.

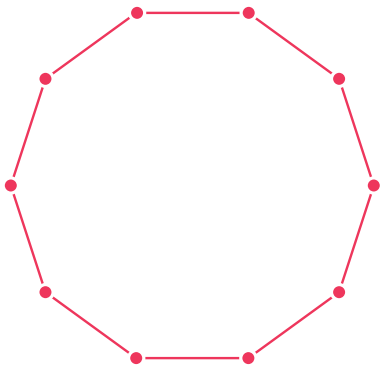

Figure 4.2: n-sided polygon

Embedded polygon

The second test case is an extended version of the simple polygon. Whereas in the simple polygon only the effect on virtual vertices could be observed by adding more vertices, also triple points can be studied. A set of vertices with a fixed locations are placed equidistant from each other on athe outer circle. These vertices are connected to the closest already existing vertices. Hence, a set of triple points is constructed, see figure 4.3.

Using the Neumann-Mullins relation (equation (4.4)), an exact solution to the change in area of the polygon is available. This will be compared with the change in area of the polygon which is embedded in the polygon constructed by the newly added vertices.

$$\frac{dA}{dt} = -2\pi M\gamma(1 - \frac{1}{6}n) \tag{4.4}$$

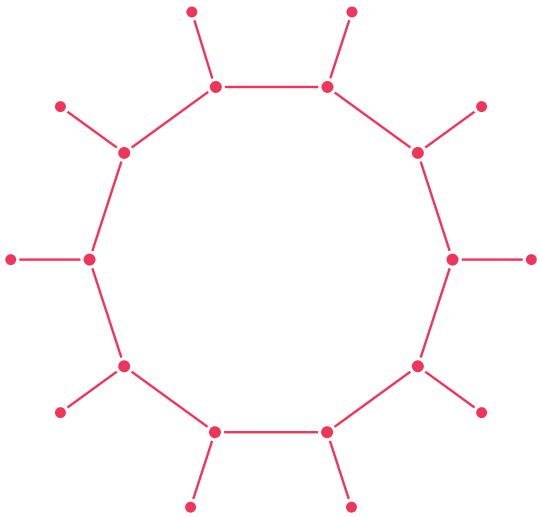

Figure 4.3: Embedded polygon, triples in the inner polygon

Embedded polygon with virtual vertices

To see the effect of adding virtual vertices, an embedded polygon is expanded with so called virtual vertices. In figure 4.4 only one extra vertex is placed between each triple point, but this number can vary (take in account the discussion in Chapter 4.1). The effect of small perturbations of the vertices can now be observed. Another interesting result would be to see what happens to the vertices when the number of triple points is six. From Neumann-Mullins the total area of the polygon should not change in time, as a hexagon is in equilibrium state.

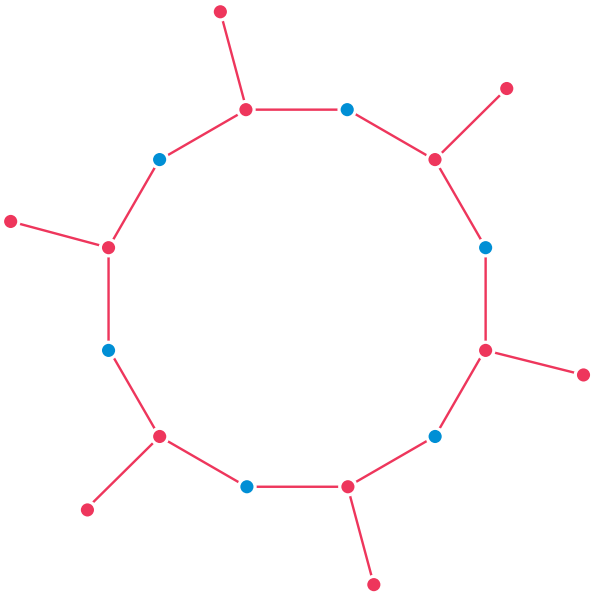

Figure 4.4: Embedded polygon with $n_{virtual} = 1$ (blue)

The final test case is implementing the chosen method from the prior three test cases on a two dimensional grid. First a 2-D Voronoi has to be constructed, then it needs to be translated such that vertex methods can use; the vertices need to be obtained from the Cellular Automata model. This has been done and a short summary of the algorithm is given in the next paragraph. Next is to check the result with the grain size distribution from Hillert [20] to see if the algorithm is correctly implemented.

Constructing periodic Voronoi and getting the triple points

1. Generate random point from which the centre of each grain is defined, a nucleus
2. Make voronoi
   - for each cell the distance $d = x^2 + y^2$ to the nucleus is calculated
   - When x or y is larger than half of the grid length
     - x = grid length $- x$
     - y = grid length $- y$
   - When $d_k < d_j$ the cell gets value belonging to nucleus i (k,j is the index of a cell)
3. Get triple
   - Define a 2x2 block from the matrix
   - Three different grains in the block are needed when it is a triple point equivalent there is one grain which has presence in 2 cells of the block. Hence, when the rows or columns are subtracted from each other the number of zeros is one or less.
4. Find neighbours of all triples
   - First list every grain belonging to the triple point
   - Find for every triple point the triple points who two grains in common and add them to neighbours
   - The coordinates of a triple point is the average over the coordinates of the cell

In figure 4.5 two examples of Voronoi diagrams are given. Either with 10 or 50 nucleation points (a '+' is used). The different colours show the different grains, a triple point is denoted by a '*'.

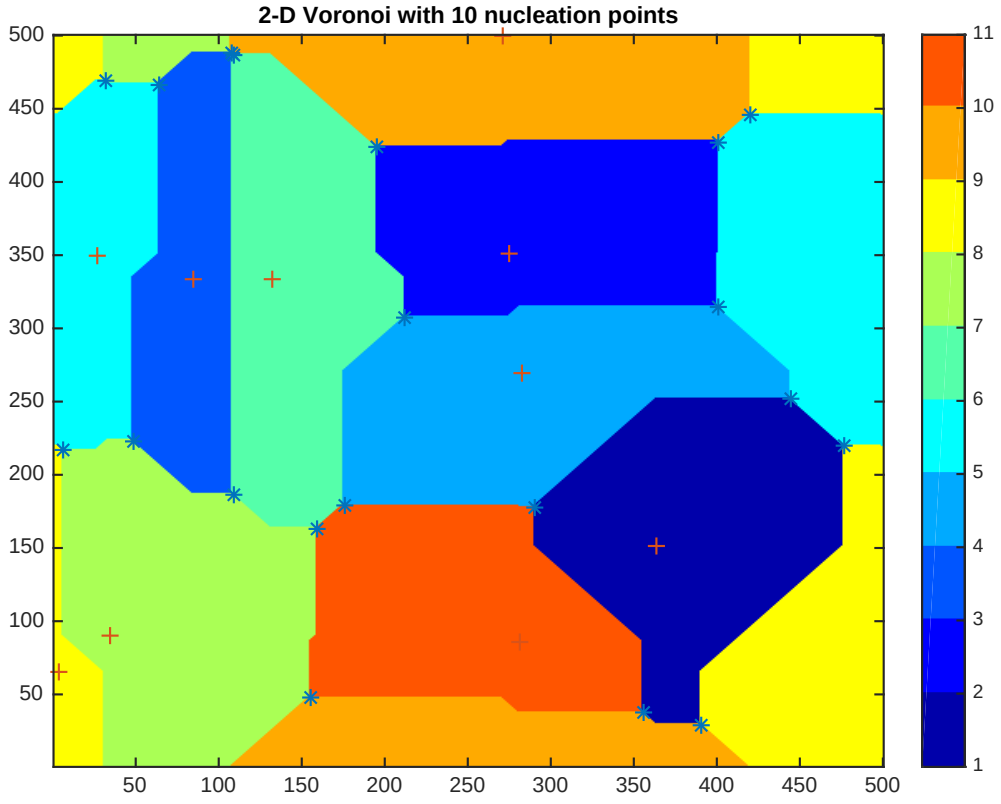

(a) Voronoi with 10 Nucleation points

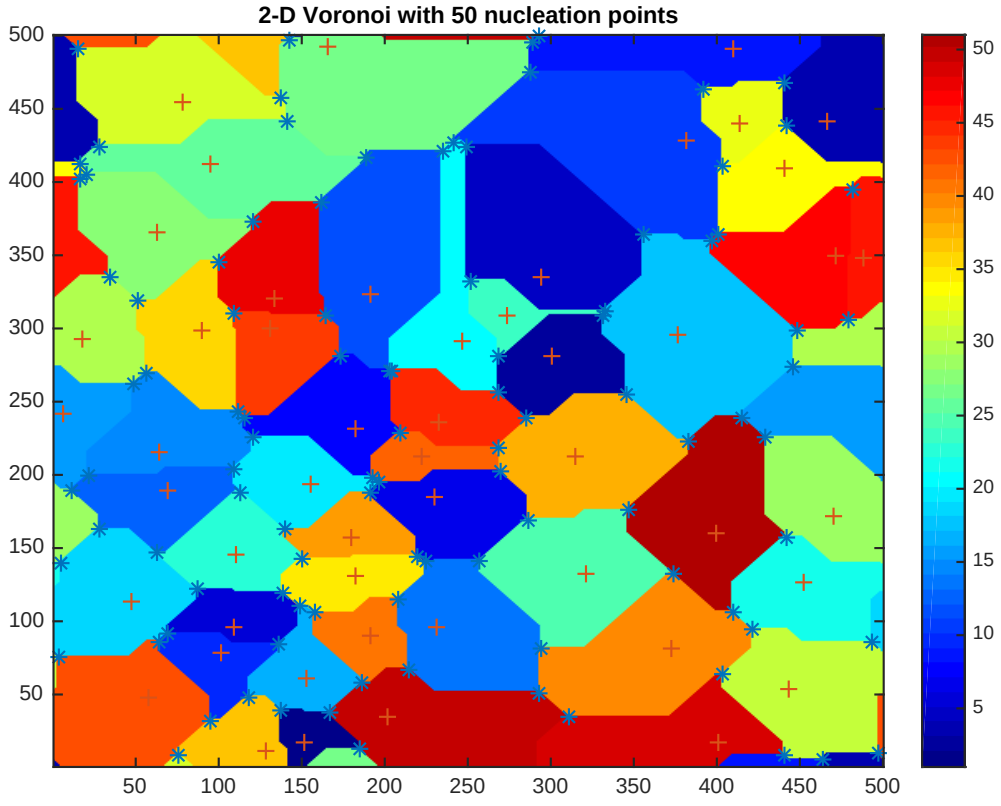

(b) Voronoi with 50 Nucleation points

Figure 4.5: Some examples of a periodic Voronoi, nucleation points (a '+' is used). The different colours show the different grains, a triple point is denoted by a '*'

5

Results

The results of the test cases introduced in Chapter four will be presented and discussed. The differences between the method first presented by Kawasaki and the method by Lazar is highlighted, such that a well reasoned decision can be made on which method to finally implement.

5.1. A simple polygon

As expected the growth of the polygon by Lazar's method is consistent with the Neumann-Mullins relation:

$$\frac{dA}{dt} = -M\gamma\frac{\pi}{3}(6-n) = -M\gamma 2\pi \tag{5.1}$$

The curvature method is nothing more then calculating the curvature based on its two neighbouring point (the essence of the method by Nippon when only virtual vertices are implemented). As seen in figure 5.1 this coincides with Kawasaki and when enough vertices are introduced it is similar to the result obtained by Lazar's method, as was expected see equation 4.3.

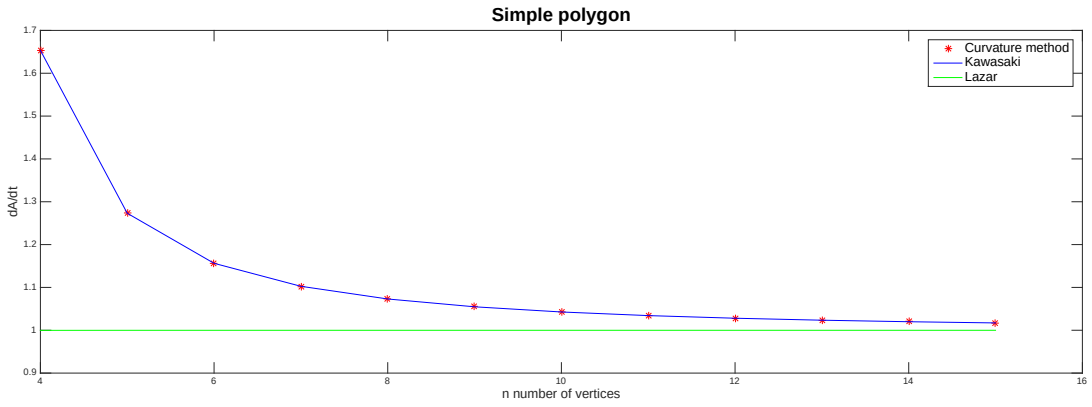

Figure 5.1: Change in area of a simple polygon, the derivative of area is multiplied by the factor $-\frac{1}{2\pi}$

5.2. Embedded polygon

The embedded polygon introduced in Chapter four is a different interpretation of the embedded polygon introduced in Weygand et al. There the virtual vertices are placed on the straight line connecting the triples. When implementing this it can be seen that figure 5.2 coincides with figure 5 of Weygand et al. However, when placing the virtuals on the circle as is done in figure 5.3 for Lazar's method, the method gives a large error when comparing to Neumann-Mullins relation. Observed can be that this is not the case for Lazar's method. When implementing the method of Nippon on the polygons and comparing with the Neumann-Mullins relation, no sensible results could be found.

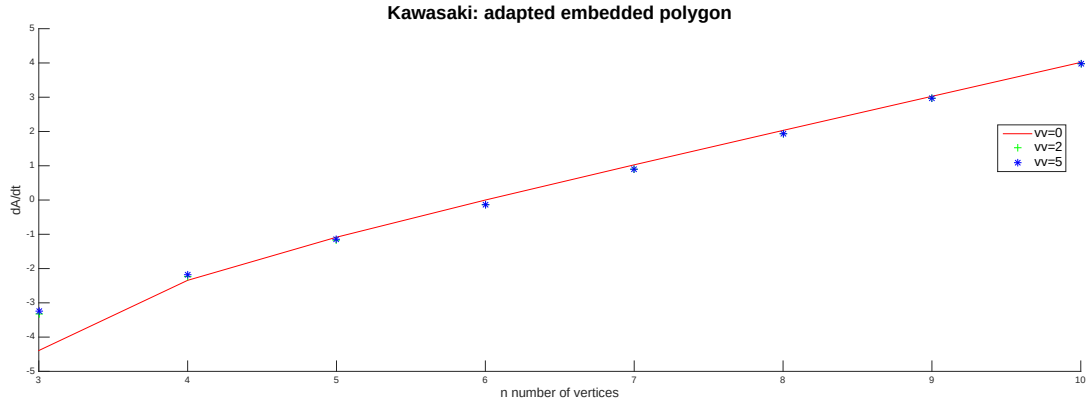

Figure 5.2: Change in area of an embedded polygon with virtual vertices (vv) on a straight line connecting the triples

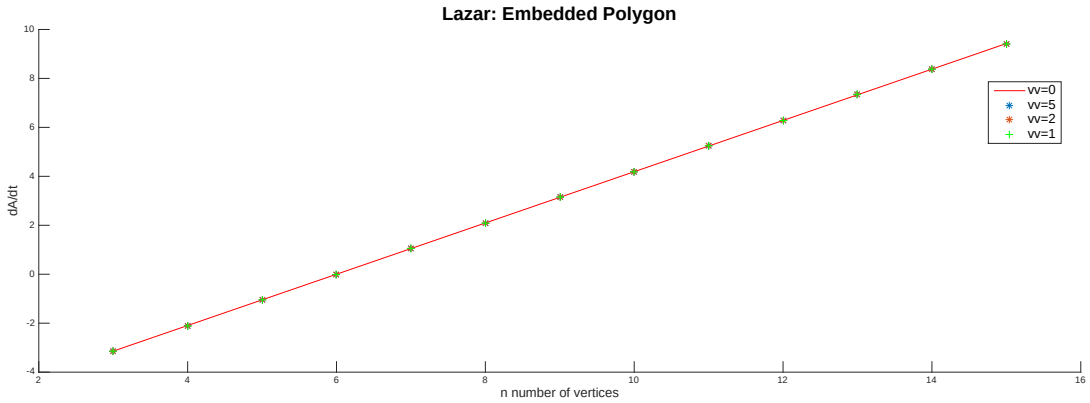

Figure 5.3: Change in area of an embedded polygon with virtual vertices (vv) on a circle connecting the triples

To illustrate what happens two figures are made of a polygon with six triple points and four virtual vertices, figures 5.4 and 5.5. Notice that the virtual points are not anymore nicely distributed over the grain boundary edge. Concluded can be that this is due to the connection of a triple point and virtual point which gives an error in the solution. This occurse because the velocity of neighbouring cells is also taken in equation (3.41). In contrast to Kawasaki the method of Lazar makes sure that the virtual points stay equidistant and the triple points move enough outside to enlarge the area which is decreased by the virtual points. This effect is not anymore present when the virtual points are given on the straight line see figures 5.6, 5.7. An overview of the obtained results is given in table 5.1.

Table 5.1: Overview of the result of the selected methods on the concerning test cases, where vv means number of virtual vertices

	Simple Polygon		Embedded Polygon Neumann-Mullins	
	Curvature	Neumann-Mullins	Arbitrary n, $vv = 0$	Arbitrary n, $vv > 0$
Nippon	+	-	-	+/-
Kawasaki	+	-	+	-
Lazar	+	+	+	+

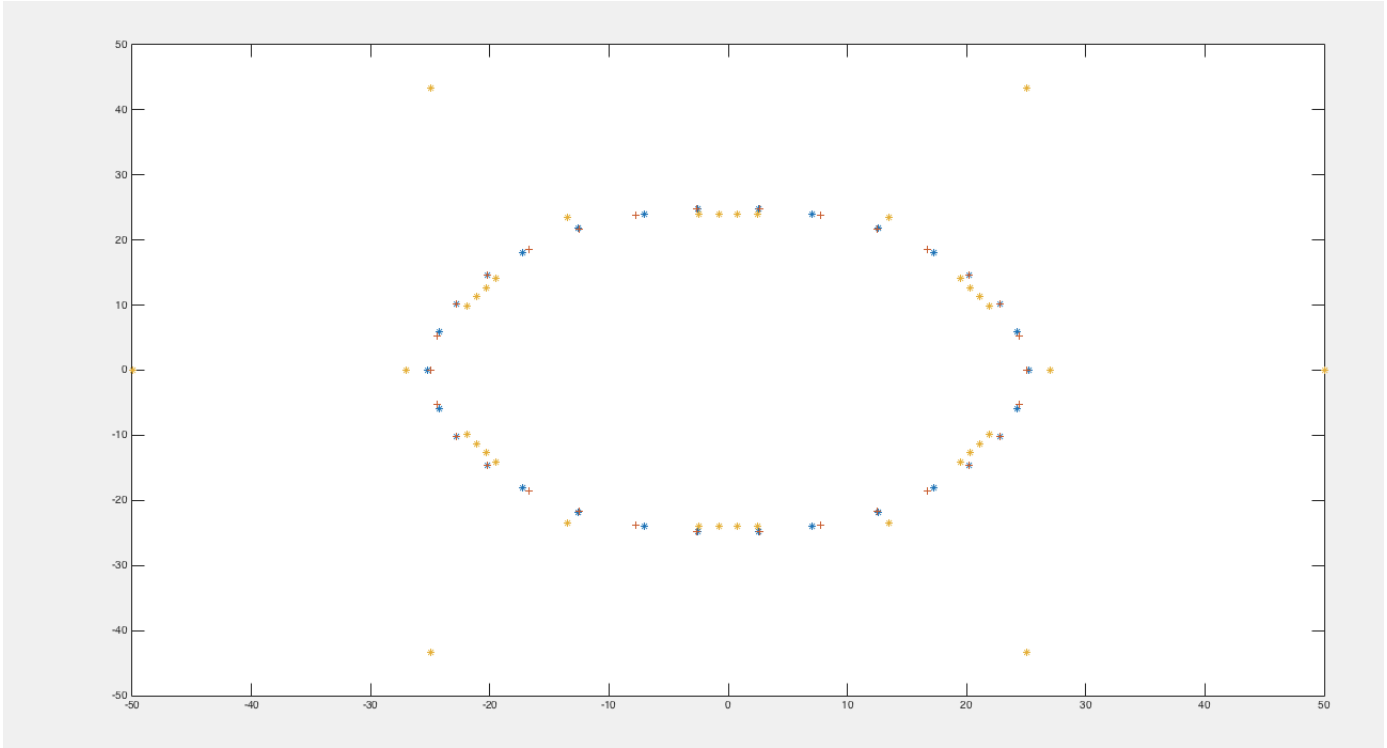

Figure 5.4: Kawasaki's method implemented on an embedded polygon with six triples and four virtual vertices, virtual vertices on the same circle. + at $t = 0$, blue * at $t = 1$, yellow * at $t = 10$.

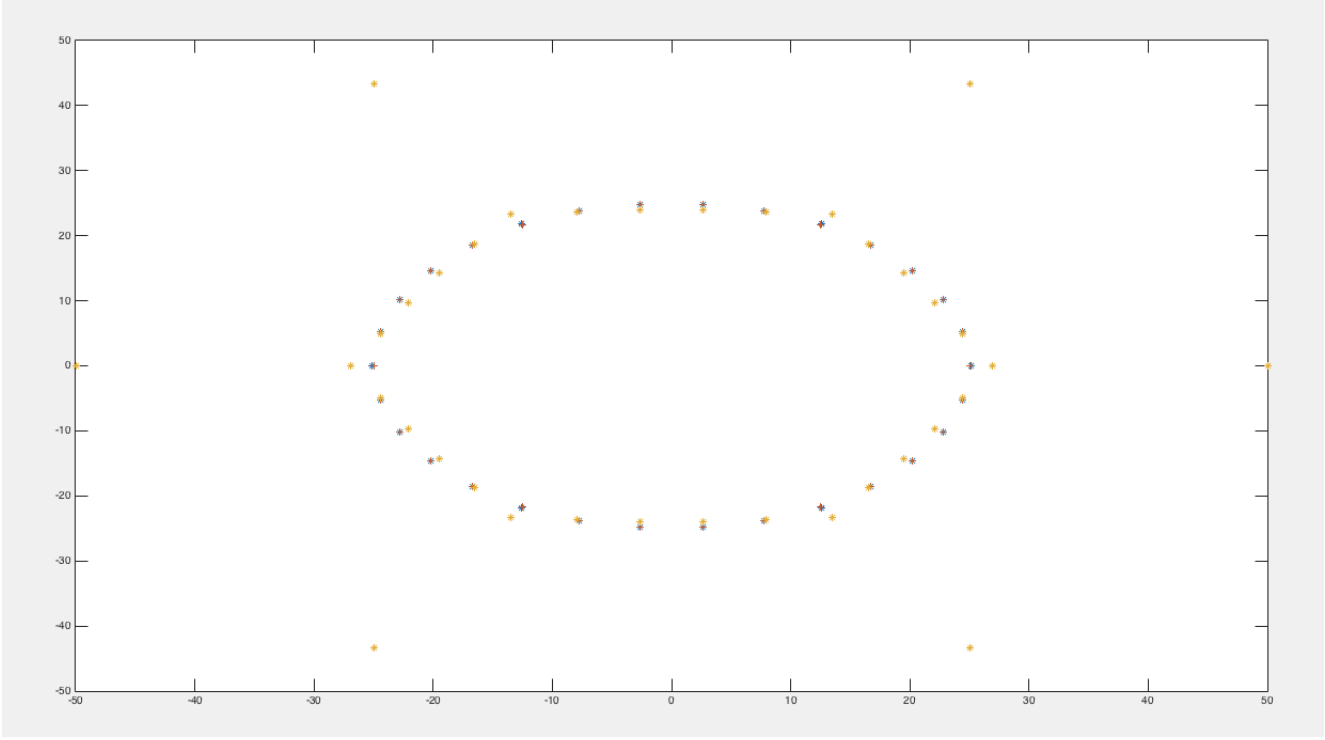

Figure 5.5: Lazar's method implemented on an embedded polygon with six triples and four virtual vertices, virtuals on the same circle. + at $t = 0$, blue * at $t = 1$, yellow * at $t = 10$.

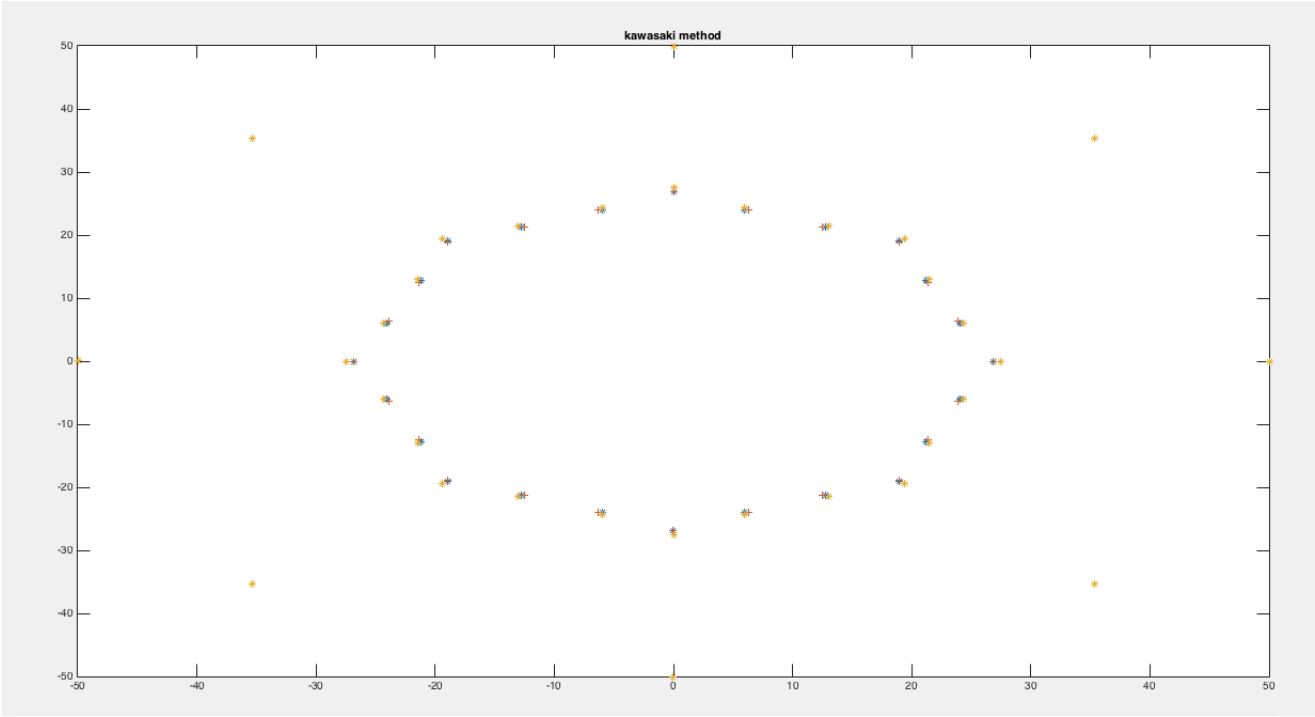

Figure 5.6: Kawasaki's method implemented on an embedded polygon with six triples and four virtual vertices, virtuals on the a straight line connecting the triples. + at $t = 0$, blue * at $t = 1$, yellow * at $t = 10$.

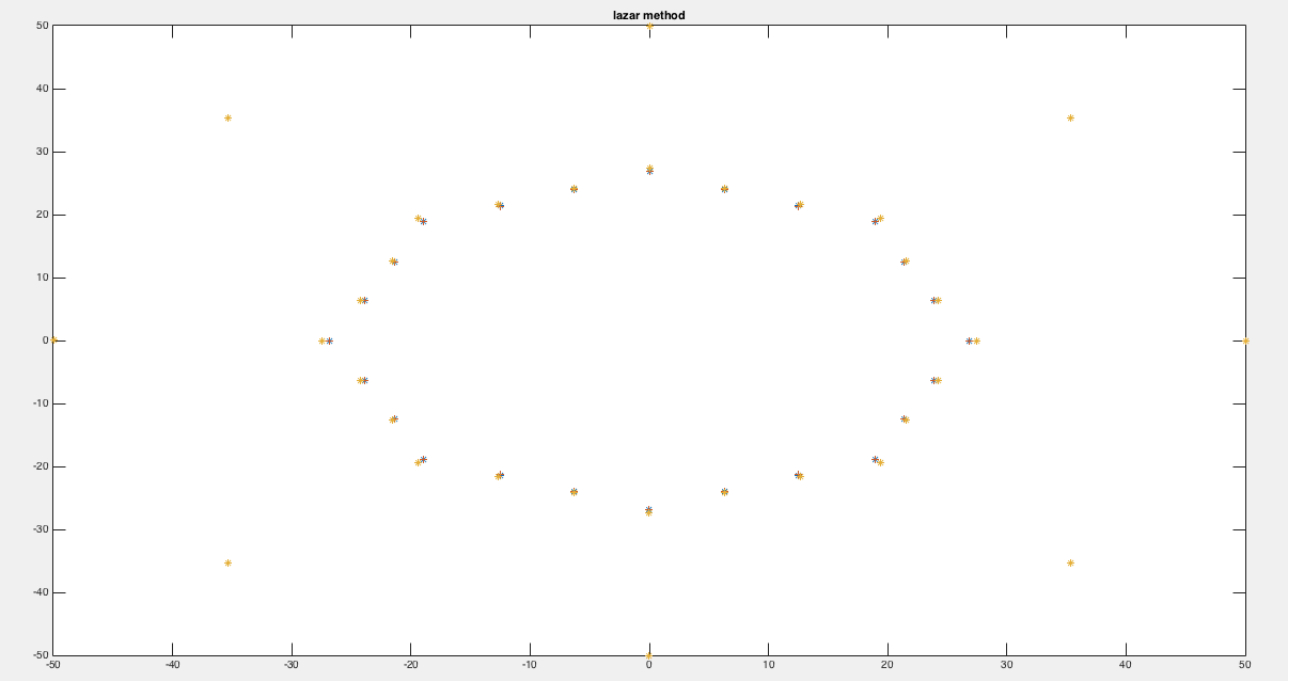

Figure 5.7: Lazar's method implemented on an embedded polygon with six triples and four virtual vertices, virtuals on the a straight line connecting the triples. + at $t = 0$, blue * at $t = 1$, yellow * at $t = 10$.

6

First conclusions & Further research

An extensive literature study has been carried out. Vertex methods have been selected to further investigate. First because from theory on metallurgy it can be concluded that the triple point has the most pronounced effect on grain growth by curvature. Second it can be observed (see Chapter 3) that curvature methods using counting cell methods are very computational costly. Another difficulty is that due to irregular boundaries the resolution of a counting cell method must be flexible which causes difficulties in the implementation.

Vertex methods have been chosen, but as the model of Bos based on cellular automata a hybrid version needs to be made. First a cellular automata model will be used and when grain growth process starts the triples points and virtual vertices need to be extracted. Next the chosen curvature method will be used. In the end when the vertices have moved, the cells of the Cellular Automata model need to be updated, such that the original model can run again.

Three vertex methods have been tested: Tamaki [32], Weygand et al. [35] and Lazar [38]. Concluding from the results of the polygon test cases, Lazars method has been chosen to further implement in a 2D and 3D structure. Next to the implementation of this method some subsequent work may be considered:

- As the derived Neumann-Mullins relation is isotropic a anisotropic relation needs to be derived
- As suggested in Chapter 2, with use of the MacPherson Srolovitz relation an improved Grain Size Distribution can be found
- A method needs to be constructed to place virtual vertex on the right spot on the boundary such that large irregularities can still be observed by the method
- Optimizing parameters e.g. the size of the time steps and the number of virtual vertices need to be found

Bibliography

[1] C.Bos, M. Mecozzi, and J. Sietsma, *A microstructure model for recrystallisation and phase transformation during the dual-phase steel annealing cycle,* Computational Materials Science , 692 (2010).

[2] D. a. Porter and K. E. Eastering, *Phase Transformations in Metals and Alloys,* , 540 (1992).

[3] *Calphad phase diagram,* http://www.calphad.com/iron-molybdenum.html, [Online; accessed 29-July-2015].

[4] *Austenite and ferrite crystal structure,* https://en.wikipedia.org/wiki/Austenite, [Online; accessed 29-July-2015].

[5] *Edge dislocation,* http://www2.warwick.ac.uk/fac/sci/physics/current/postgraduate/regs/mpags/ex5/strainedlayer/disloc1/, [Online; accessed 29-July-2015].

[6] *Screw dislocation,* https://www.nde-ed.org/EducationResources/CommunityCollege/Materials/Structure/linear_defects.html, [Online; accessed 29-July-2015].

[7] *Dislocation annihilated,* http://users.encs.concordia.ca/~mcqueen/Dislocations_lecture8.html, [Online; accessed 29-July-2015].

[8] J. Czochralski, Int. Z. Metallogr. , 289 (1914).

[9] J. Ewing and W. Rosenhain, Phil. Trans. roy. Soc. A , 353 (1900).

[10] C. Benedicts, Kolloid Zeitschr. , 217 (1940).

[11] W. Bragg, Proc. Phys. Soc. , 105 (1940).

[12] C. Smith, *Private communication,* .

[13] J. Burke and D. Turnbull, *Recrystallization and grain growth,* Progress in Metal Physics , 220 (1952).

[14] *Surface tension Young-Laplace,* https://simple.wikipedia.org/wiki/Surface_tension, [Online; accessed 29-July-2015].

[15] K. Aust and B. Chalmers, Proc. roy. Soc. , 210 (1950).

[16] C. Dunn, F. Daniels, and M. Bolton, Trans. Amer. Inst. min. (metall.) Engrs , 338 (1950).

[17] E. A. Lazar, *The Evolution of Cellular Structures via Curvature Flow*, Ph.D. thesis, Princeton University (2011).

[18] M. Gage and R. Hamilton, *The heat equation shrinking convex plane curves,* .

[19] M. Grayson, *The heat equation shrinks embedded plane curves to round points,* .

[20] M. Hillert, *On the theory of normal and abnormal grain growth,* Acta Metallurgica , 227 (1965).

[21] W. W. Mullins, *Two-Dimensional Motion of Idealized Grain Boundaries,* Journal of Applied Physics , 900 (1956).

[22] R. D. MacPherson and D. J. Srolovitz, *The von Neumann relation generalized to coarsening of three-dimensional microstructures.* Nature , 1053 (2007).

[23] *Theory, Algorithms, and Applications of Level Set Methods for propogating Interfaces,* `//math.berkeley.edu/~sethian/2006/Papers/sethian.actanumerica.1995.pdf` (), [Online; accessed 29-July-2015].

[24] *Level set explained by sethian,* `math.berkeley.edu/~sethian/2006/Semiconductors/ieee_level_set_explain.html` (), [Online; accessed 29-July-2015].

[25] S. Kim and D. I. Kim, *Computer simulations of two-dimensional and three-dimensional ideal grain growth,* .

[26] K. Janssens, *An introductory review of cellular automata modeling of moving grain boundaries in polycrystalline materials,* Mathematics and Computers in Simulation , 1361 (2010).

[27] M. M. Mul, *Modeling the austenite ferrite transformation by cellular automaton, improving interface stability*, Ph.D. thesis, TU Delft (2014).

[28] L. Wei, X. Lin, M. Wang, and W. Huang, *Low artificial anisotropy cellular automaton model and its applications solidification to the transition in directional,* .

[29] L. Wei, X. Lin, M. Wang, and W. Huang, *A cellular automaton model for the solidification of a pure substance,* , 123 (2011).

[30] S. J. Cummins, M. M. Francois, and D. B. Kothe, *Estimating curvature from volume fractions,* , 425 (2005).

[31] M. Williams, Ph.D. thesis.

[32] T. Tamaki, *Two-dimensional Grain Growth Simulation by Local Curvature Multi-vertex Model,* , 31 (2013).

[33] R. Fullman, *Metal interfaces,* .

[34] A. S. J. van Kan and F. Vermolen, *Numerical methods in scientific computing,* VSSD (2005).

[35] Y. B. J. Lepinoux, D.Weygand, *A vertex dynamics simulation of grain growth in two dimensions,* Philosophical Magazine B , 329 (1998).

[36] K. Fuchizaki, T. Kusaba, and K. Kawasaki, *Computer modelling of three-dimensional cellular pattern growth,* Philosophical Magazine Part B , 333 (1995).

[37] K. Kawasaki, T. Nagai, and K. Nakashima, *Vertex models for two-dimensional grain growth,* Philosophical Magazine Part B , 399 (1989).

[38] E. a. Lazar, R. D. MacPherson, and D. J. Srolovitz, *A more accurate two-dimensional grain growth algorithm,* Acta Materialia , 364 (2010).

[39] E. a. Lazar, J. K. Mason, R. D. MacPherson, and D. J. Srolovitz, *A more accurate three-dimensional grain growth algorithm,* Acta Materialia , 6837 (2011).